Title: TKI-conditioned immunotherapy using *uv*-inactivated reovirus promotes survival in hepatocellular carcinoma, mediated by cytotoxic CD4$^+$ T-cells

Authors: Russell Hughes[1]*, Amy Moran[1], Karen J. Scott[1], Elizabeth Appleton[1], Matthew J. Bentham[1], Elizabeth Ilett[1], Alan Melcher[3], Andrew Macdonald[2], Adel Samson[1,]*, and Stephen Griffin[1,]*

Affiliations:

[1]Leeds Institute of Medical Research, St. James's University Hospital, University of Leeds; Leeds, UK.

[2]School of Molecular and Cellular Biology, Faculty of Biological Sciences, University of Leeds; Leeds, UK.

[3]The Institute for Cancer Research, University of London; London, UK.

*Corresponding author(s): s.d.c.griffin@leeds.ac.uk; a.samson@leeds.ac.uk; r.hughes1@leeds.ac.uk

ABSTRACT

Hepatocellular carcinoma (HCC) is the third most common cause of cancer deaths worldwide. Whilst immunotherapy combination regimens are now standard of care for advanced HCC, tyrosine kinase inhibitors (TKIs), such as the former first-line agent sorafenib, remain an important choice for those unable to tolerate immunotherapies but provide marginal efficacy. Therefore, we sought to determine whether the efficacy of sorafenib could be enhanced by combining it with human *Orthoreovirus*, an oncolytic virus possessing immunostimulatory properties. We discovered that *uv*-inactivated, replication-deficient reovirus, not live virus, significantly extended the survival of mice bearing HCC tumors when combined with

sorafenib. This response was characterised by increased intra-tumoral expression of both CCL5 and IFNB, and a skewing of the T-cell ratio in favor of non-canonical, $CD4^+$ cytotoxic T-cells expressing granzyme B, but *not* perforin. This study highlights both the therapeutic potential of *uv*-reovirus in TKI-conditioned HCC and the often-overlooked contributions of non-classical immune mechanisms to therapeutic success.

One sentence summary: A unique therapy combining TKI-conditioning and *uv*-inactivated reovirus suppresses the growth of hepatocellular carcinomas, mediated by $GZMB^+CD4^+$ cytotoxic T-cells.

35 **INTRODUCTION**

36

37 Hepatocellular carcinoma (HCC) is the third leading cause of cancer deaths worldwide.
38 A significant proportion of HCC patients (~40%) present with advanced disease at diagnosis,
39 excluding them from potentially curative surgical interventions. Consequently, ~88% of
40 patients succumb to the disease within 5-years post-diagnosis across disease stages. Systemic
41 treatment options for patients with advanced HCC have greatly advanced in recent years, with
42 combination regimens involving immune checkpoint inhibitors (ICIs) now being standard of
43 care. However, a significant proportion of patients are unable to tolerate ICI therapy, such as
44 those with pre-existing autoimmune disease, for these patients, systemic treatment options are
45 limited to TKI therapy, most commonly sorafenib (Nexavar^{TM}, Bayer/Onyx). The principle
46 cellular targets for sorafenib are the receptor TKs VEGFR and PDGFR, and certain Raf family
47 serine/threonine kinases. However, sorafenib also displays significant off-target effects (*1*) and
48 has immunosuppressive properties (*2, 3*). The survival benefit gained following sorafenib
49 treatment is limited (*4*), thus, considerable need exists for new approaches that augment TKI
50 efficacy to improve both survival and quality-of-life outcomes for patients.

51

52 Oncolytic viruses (OV) are a promising area of cancer immunotherapy and can be well
53 tolerated in patients, even those with pre-existing autoimmune disease. Numerous OVs are in
54 clinical trials for a range of solid and hematological malignancies. OV-therapies are known to
55 exert their anti-cancer activity *via* two global mechanisms. Firstly, direct tumor cell lysis:
56 malignant cells frequently accumulate defects in innate anti-viral pathways, which, coupled
57 with an enhanced rate of cell proliferation, creates a favorable environment for unrestricted
58 viral replication leading to apoptotic cell death and lysis. Secondly, stimulation of anti-tumor
59 immunity arises due to direct leukocyte stimulation, and the liberation of PAMPs, DAMPs and

60 other cell components including tumor antigens (either tumor-associated or tumor-specific),
61 following immunogenic cancer cell death. The balance between how these processes combine
62 to achieve efficacy logically varies according to both the OV, as well as the tumor in question.
63
64 Oncolytic human *Orthoreovirus* ("Reo": type-3, Dearing Strain, marketed as "Pelareorep",
65 [REOLYSIN^{TM}] by Oncolytics Biotech, Calgary) has been both widely and safely used in
66 numerous patient studies and is currently under fast-track review for both metastatic breast
67 cancer and advanced/metastatic pancreatic cancer (*5*). Although Reo exerts direct lytic effects
68 on cancerous cells, there is considerable interest in its ability to activate the immune system (*6-*
69 *14*). Host cells possess a variety of sensory mechanisms for the detection and prevention of
70 viral infection. These innate sensors are triggered in response to PAMPs common to most
71 viruses, such as nucleic acids. Reo harbors a segmented dsRNA genome that can be detected
72 by both endosomal Toll-like receptors (TLR3) and cytosolic RIG-like receptors (RIG-I and
73 MDA-5). Upon activation, these viral sensors trigger host cells to produce a wide variety of
74 inflammatory cytokines, but key among them are interferons. These potent mediators induce
75 an anti-viral state in neighbouring cells by upregulating the expression of interferon-stimulated
76 genes (ISGs), thereby limiting virus replication and spread. Importantly, interferons also
77 stimulate and enhance adaptive immune cell function, resulting in the neutralization of viral
78 particles and killing of infected cells. In the context of cancer, Reo can stimulate both dendritic
79 cell maturation (*7, 11*) and increase antigen exposure in infected tumor cells (*9, 10*). Together,
80 these promote the generation of antigen-specific cytotoxic $CD8^+$ T-cell responses capable of
81 breaking tumor immune tolerance in pre-clinical mouse models (*9, 10*). Immune activation is
82 also observed in patients treated with Reo as evidenced by increased expression of the
83 interferon gamma-inducible immune checkpoint molecule PD-L1 (*15*), increased levels of anti-

84 Reo neutralizing antibodies in peripheral blood (*16-20*), and the accumulation of intra-tumoral
85 T-cells (*21*).
86
87 $CD4^+$ T-helper cells (T_H-cells) are a critical component of the adaptive arm of the immune
88 system. As such, $CD4^+$ T_H-cells have diverse roles, including enhancing the functions of innate
89 immune cells and facilitating both cell-mediated and humoral responses against infectious
90 microorganisms and malignant cells. Despite their role as master co-ordinators, T_H-cells can
91 also exert direct toxicity against a range of cell types, under specific conditions. Cytotoxic
92 $CD4^+$ T_H-cells (CTHs) are frequently observed in patients with chronic viral infections, such
93 as human cytomegalovirus (hCMV) (*22-25*), hepatitis B, C and D viruses (*26*), human
94 immunodeficiency virus (HIV) (*27*) and Epstein-Barr virus (EBV) (*28-31*), and in pre-clinical
95 mouse models of lymphocytic choriomeningitis (LCMV) and gamma herpes virus infection
96 (MHV68) (*32, 33*). CTHs are characterised by co-expression of granzyme B and perforin,
97 reminiscent of *bona fide* cytotoxic $CD8^+$ T-cells (CTLs), although they instead utilise an
98 MHCII-dependent, antigen-specific mode of target cell killing. T_H-cells also deploy a range of
99 granzyme/perforin-independent modes of cytotoxicity, including FasL/Fas and TNF-related
100 apoptosis-inducing ligand (TRAIL), which are involved in the maintenance of peripheral
101 tolerance through activation-induced cell death (AICD) and the elimination of malignant or
102 virus-infected cells (*34-36*).
103
104 Here, we show that combining a *uv*-inactivated, replication-deficient Reo (*uv*-Reo) with the
105 targeted agent sorafenib dramatically extended the survival of mice bearing syngeneic HCC
106 tumors compared to the use of live Reo (Reo) in the same combination. Furthermore, the
107 combination of *uv*-Reo with sorafenib induced a T_H1-dominated anti-tumor immune response
108 underpinned, surprisingly, by multiple antigen-*independent* modes of killing. This multi-

109 faceted response involved tumor-borne expression of the T_H1-cell tropic chemokine, CCL5,
110 leading to a markedly increased CD4:CD8 ratio amongst tumor-infiltrating lymphocytes (TIL).
111 Ensuing production of TNFA and IFNG by T_H1-cells mediated paracrine tumor cell killing,
112 enhanced by sorafenib-induced sensitisation of HCC cells to death upon exposure to these
113 cytokines. The crucial remaining aspect of this response involved the therapy-induced
114 expression of IFNB, which engaged a proximity-dependent mode of killing in T_H1-cells that
115 was reliant on granzyme B, but neither perforin, nor MHCII. This study highlights the unique
116 immune mechanisms of *uv*-inactivated reovirus as an immunotherapeutic approach to enhance
117 the efficacy of sorafenib during the treatment of HCC.

118 **RESULTS**

119

120 **Suppression of HCC tumor growth during uv-Reo/sorafenib therapy involves the skewing**
121 **of intra-tumoral T-cell ratios (T_H:CTL) in favor of $CD4^+$ T_H-cells.**

122 We investigated the therapeutic effect of combining sorafenib with Reo in Balb/c mice
123 bearing syngeneic, subcutaneous 1MEA HCC tumors, controlling for virus-mediated effects
124 by including *uv*-inactivated virus (*uv*-Reo – *i.e.,* replication deficient). Reo and other
125 monotherapies produced a small, albeit statistically significant survival advantage. However,
126 when combined with sorafenib, *uv*-Reo substantially increased the survival of tumor-bearing
127 mice (**Fig. 1A,** *right panel*). This was not the case for Reo combined with sorafenib (**Fig. 1A,**
128 *left panel*). The therapeutic benefit of *uv*-Reo/sorafenib in combination was greatly reduced in
129 SCID mice, yet completely lost in SCID/Beige mice, supporting an immune-mediated
130 mechanism driven primarily by the adaptive response (**Fig. 1B**).

131 Thus, we examined the leukocyte composition of 1MEA tumors, grown in
132 immunocompetent Balb/c hosts, but this time harvested when responding to therapy (Therapy
133 phase – **Fig 1A,** *top panel*), to identify changes in infiltrating immune cell(s) that contribute to
134 the subsequent improved survival phenotype. A robust increase in $CD3^+CD8^+$ CTLs was
135 apparent in HCC tumors treated with Reo (monotherapy, and in combination with sorafenib)
136 (**Fig. 2A & C**). Nevertheless, based upon the survival phenotype (**Fig. 1A**), these CTLs alone
137 were unable to retard tumor growth long-term and adequately extend survival. *uv*-Reo
138 monotherapy failed to elicit a significant change in frequency for any leukocyte populations
139 investigated (**Fig. S1**). However, when combined with sorafenib, *uv*-Reo increased the
140 abundance of $CD3^+CD4^+$ T_H-cells, but not $CD3^+CD8^+$ CTLs (**Fig. 2A - C**). This significantly
141 skewed the T-cell ratio in favor of $CD4^+$ cells (**Fig. 2D**) implying that the response to therapy
142 that underpinned the ensuing improved survival was dominated by T_H-cells.

143 We performed a cytokine array analysis to better understand how *uv*-Reo/sorafenib
144 therapy altered the cytokine milieu of the tumor microenvironment (**Fig. S2A**). We discovered
145 that elevated levels of intra-tumoral IFNG and TNFA mirrored the pattern of increased
146 abundance of $CD3^+CD4^+$ T-cells (**Fig. 3A**). These cytokines are known to be expressed by T_H1-
147 activated T-cells and, accordingly, were expressed within the tumor-infiltrating $CD3^+CD4^+$
148 cells in mice treated with *uv*-Reo/sorafenib therapy, as determined by flow cytometry (**Fig.**
149 **3B**). By contrast, levels of cytokines associated with T_H2 and T_H17 T-cell subsets did not mirror
150 the pattern of $CD4^+$ T-cell recruitment (**Fig. S2B**).
151 We also observed elevated levels of the chemokine CCL5 coincident with the increased
152 abundance of $CD3^+CD4^+$ T-cells (**Fig. 3C**). *In vitro*, the expression of CCL5 by human and
153 murine HCC cells was significantly increased by treatment with *uv*-Reo compared to Reo, even
154 in the presence of sorafenib (**Fig. S2C - D**). CCL5 exerts a potent chemotactic effect on T_H1-
155 cells, but not naïve $CD4^+$ T-cells, and a specific small molecule inhibitor supported that this
156 chemotaxis is mediated by the CCR5 chemokine receptor (**Fig. 3D**). This was readily detected
157 on the surface of T_H1-activated T-cells *in vitro,* and on $CD3^+CD4^+$ T-cells in mouse tumors
158 treated with *uv*-Reo/sorafenib (**Fig. 3E**). These data indicate that the combination of *uv*-Reo
159 and sorafenib exerts a suppressive effect on continuing HCC growth by skewing the intra-
160 tumoral T-cell ratio in favor of $CD4^+$ T_H1-cells, not $CD8^+$ CTLs.
161
162 **T_H1-activated $CD4^+$ T-cells exert contact-independent tumoricidal activity against HCC**
163 **cells via a TNFA-dependent mechanism.**
164
165 We co-cultured HCC cells with $CD4^+$ T-cells to determine whether the latter possessed
166 anti-tumor properties. T_H1-cells, but not naïve $CD4^+$ T-cells, displayed measurable tumoricidal
167 activity (**Fig. 4A**). However, target cell killing also occurred when the two cell types were

168 physically separated, demonstrating that a soluble factor was in part responsible (**Fig. 4B**).
169 Thus, we examined the tumoricidal activity of soluble mediators released by T_H1-cells known
170 to have cytotoxic properties, beginning with IFNG (*37, 38*). Exposure of human and mouse
171 HCC cells to increasing concentrations of IFNG failed to induce detectable toxicity (**Fig. S3A**).
172 However, pre-treatment of HCC cells with IFNG sensitised them to killing by T_H1-cells,
173 demonstrating that an additional soluble factor was involved (**Fig. S3B**). Next, we treated HCC
174 cells with sorafenib, using a clinically relevant dose, prior to exposure to increasing
175 concentrations of IFNG. Sorafenib is known to increase cancer cell sensitivity to a range of
176 death-inducing mediators *via* modulation of intra-cellular death pathways (*39, 40*), so we
177 hypothesised that sorafenib might sensitise HCC cells to IFNG. Sorafenib increased the
178 responsiveness of HCC cells to T_H1-mediated killing (**Fig. S3C**) in co-culture assays but did
179 so by sensitising them to a soluble mediator other than IFNG (**Fig. S3D**). Next, we discovered
180 that addition of TNFA-neutralizing antibodies to co-culture assays inhibited T_H1-mediated
181 HCC killing dose dependently (**Fig. 4C**). Antibody blockade of cancer cell killing was not
182 observed for other T_H1-derived cytotoxic mediators, such as TRAIL or LTA (**Fig. S3E – F**),
183 demonstrating that TNFA was the dominant soluble effector molecule. Thus, we added
184 recombinant TNFA to HCC cultures and found that it was directly cytotoxic (**Fig. 4D**).
185 Furthermore, this toxicity was significantly enhanced by prior treatment with either IFNG or
186 sorafenib (**Fig. 4E**); the same was also true for mouse HCC cells (**Fig. 4F**). Together, these data
187 demonstrated that TNFA was the dominant soluble mediator of T_H1-cellular cytotoxicity
188 towards HCCs, with a sensitising role for both IFNG and sorafenib. However, because T_H1-
189 cells were not exclusively recruited into tumors treated with *uv*-Reo/sorafenib therapy, we
190 reasoned that additional mechanisms likely enhance tumor killing for this particular treatment
191 combination.

192 **IFNB induces a close-contact antigen-independent tumoricidal activity in T_H1-cells**
193 **mediated by granzyme B in the absence of perforin.**

194 Type-I interferons are important mediators of anti-viral immunity *via* upregulation of
195 interferon-stimulated genes (ISGs), as well as enhancing immune-mediated killing of infected
196 cells. We, and others, have shown that Reo and *uv*-Reo are potent inducers of the type-I
197 interferon, 'IFNB' (*11, 41*) particularly in the context of both HCC and primary liver tissue
198 (*41*). Thus, we compared the levels of IFNB produced by both human and mouse HCC cells
199 *in vitro,* and mouse tumors *ex vivo,* when treated with Reo/*uv*-Reo monotherapy or in
200 combination with sorafenib. Human and mouse HCC cells responded to *uv*-Reo (alone and in
201 combination with sorafenib) with a robust induction of IFNB expression, which, surprisingly,
202 was significantly larger than the response to Reo (**Fig. 5A - B**), consistent with the expression
203 pattern seen for CCL5, *in vitro* (**Fig. S2C - D**). We examined the intracellular signalling events
204 in HCC cells treated with Reo/*uv*-Reo alone and in the presence of sorafenib to better
205 understand the differential induction of IFNB. The transcription factors NF*k*B p65 (RELA)
206 and IRF3 were phosphorylated to a greater extent in HCCs treated with *uv*-Reo compared to
207 Reo, both in the presence and absence of sorafenib, as determined by Western blot (**Fig. S4A**).
208 Therefore, we compared the contribution made by each of these factors to the expression of
209 IFNB using luciferase reporter assays containing either IRF3 (PD116) or NF*k*B p65 (PRDII)
210 binding elements from the IFNB promoter. The IRF3 reporter was more strongly activated in
211 HCC cells infected with *uv*-Reo (in both the presence and absence of sorafenib) compared to
212 Reo (**Fig. S4B**). However, the opposite was true for the NF*k*B reporter with more robust
213 activation in the presence of Reo, not *uv*-Reo (**Fig. S4C**). These data indicated that the
214 differential activation and functional output from these pathways contributed the difference in
215 IFNB induction by Reo/*uv*-Reo.

216 Viruses dedicate considerable proportions of their coding capacity towards the production of
217 virulence factors that minimise the interferon response within infected cells. Reovirus is no
218 exception (*42, 43*) so we hypothesised this may account for the differential induction of IFNB
219 observed in HCC cells. Consistently, infecting HCC cells with Reo prior to *uv*-Reo
220 significantly dampened the induction of IFNB compared to *uv*-Reo alone (**Fig. S4D**). In
221 addition, the kinetics of virus-induced IFNB expression were slower with Reo compared to *uv*-
222 Reo, indicating a delay in viral sensing (**Fig. S4E**). Critically, this effect was dependent upon
223 Reo replication, and so presumably gene expression, as a nucleotide analogue inhibitor of the
224 RNA-dependent RNA polymerase, 2'-C-methylcytidine, ameliorated the suppressive effect
225 (**Fig. S4D**). These data indicated that a virulence factor could account for the differential
226 induction of IFNB between Reo and *uv*-Reo, *in vitro*. Accordingly, Reo μNS protein is known
227 to redirect IRF3 to viral replication factories (*42*), consistent with decreased levels of
228 phosphorylated protein within Reo infected HCC cells (**Fig. S4A**). Thus, whilst attenuation of
229 the Type 3 Dearing strain may be severe compared to other *Orthoreoviruses*, it is by no means
230 absent.

231 Interestingly, the highest level of intra-tumoral IFNB was found in tumors from mice
232 treated with *uv*-Reo/sorafenib therapy (**Fig. 5C**), suggesting that IFNB might play an important
233 mechanistic role in suppressing tumor growth. Thus, we added recombinant IFNB to co-
234 culture assays comprising HCC cells and T_H1-cells to determine how this affected target cell
235 killing. IFNB significantly enhanced the tumoricidal activity of T_H1-cells (**Fig. 5D**) but, unlike
236 IFNG or sorafenib, did so *via* a mechanism that required proximity between the two cell types.
237 Separation of human or mouse IFNB-stimulated T_H1-cells from target HCC cells reduced
238 killing to the level of untreated T_H1-cells (**Fig. 5E**). Next, we examined the effect of pre-
239 treating HCC target cells with IFNB to determine whether the enhanced killing was a
240 consequence of either increased target cell sensitivity or the increased killing capacity of T_H1-

241 cells. Consistent with the latter, target cell killing was only enhanced when IFNB was added
242 concurrently with T_H1-cells (**Fig. 5F**) demonstrating that the IFNB acted directly on $CD4^+$ T-
243 cells.

244 We next investigated potential mediators of IFNB-enhanced T_H1-mediated killing of
245 HCC cells, namely TNF-related apoptosis-inducing ligand (TRAIL) and FasL/Fas, both of
246 which are known to be utilised by T_H-cells in a juxtacrine manner. IFNB induced dose-
247 dependent expression of both soluble, and membrane-bound TRAIL in T_H1-cells, but not in
248 naïve $CD4^+$ T-cells (**Fig. S5A – C**). However, addition of a TRAIL-neutralizing antibody to
249 co-culture assays did not inhibit IFNB-enhanced T_H1-mediated killing (**Fig. S5D**). Similarly,
250 surface FasL expression was induced in $CD4^+$ T-cells upon T_H1-activation, and the Fas receptor
251 was readily detectable on HCC targets. However, FasL expression was not further enhanced
252 upon treatment with IFNB (**Fig. S5E - F**) and the addition of Fas neutralizing antibodies to co-
253 culture assays also failed to diminish IFNB-enhanced HCC killing (**Fig. S5G**). Consequently,
254 we considered the involvement of MHCII-dependent degranulation, described previously for
255 cytotoxic $CD4^+$ T-cells (*44, 45*). However, MHCII was not detected on human or mouse HCC
256 targets, and again addition of MHCII-neutralizing antibody to co-culture assays had no effect
257 (**Fig. 6A - B**).

258 Despite the lack of MHCII involvement, addition of EGTA (a calcium chelating
259 inhibitor of degranulation) to co-culture assays dose-dependently inhibited IFNB-enhanced
260 target cell killing (**Fig. 6C**). Hence, we next quantified the proportion of $CD4^+$ T-cells with
261 surface expression of the degranulation marker CD107a and intra-cellular expression of both
262 granzyme B and perforin, important components of the apoptosis-inducing machinery
263 deployed by cytotoxic T-cells. Using both human and mouse $CD4^+$ T-cells, we observed a
264 marked increase in the proportion of T-cells with surface CD107a expression and intra-cellular
265 granzyme B (GZMB) following T_H1-activation. Furthermore, this expression was significantly

266 enhanced upon stimulation with IFNB, consistent with the additive enhancement of killing by
267 these treatments (**Fig. 6C – D**). GZMB was also abundant in supernatants from T_H1-activated
268 T-cells, and levels were further increased upon treatment with IFNB (**Fig. 6F**). Accordingly,
269 addition of a small molecule GZMB inhibitor to co-culture assays dose dependently inhibited
270 IFNB-enhanced killing (**Fig. 6G** – *left panel*). The same response was also seen in the presence
271 of a pan-caspase inhibitor (**Fig. 6G** – *right panel*). Interestingly, only 1% of T_H1-cells treated
272 with IFNB expressed perforin (PRF) and this was only at low levels (**Fig. S6A**). Perforin was
273 undetectable in naïve $CD4^+$ T-cells. Taken together, these data demonstrate that IFNB induces
274 an antigen/perforin-independent mode of HCC cell killing, involving the short-range release of
275 GZMB by T_H1-cells.

276 Finally, given that $CD8^+$ cells were also present within tumors treated with *uv*-Reo and
277 sorafenib (**Fig. 2**), we compared their ability to engage in antigen-independent HCC killing
278 with that of $CD4^+$ T-cells. Consistent with the notion that $CD8^+$ T-cells played a lesser role in
279 tumor response to therapy, whilst they could indeed kill HCCs upon activation and this was
280 further enhanced by IFNB, their tumoricidal activity was significantly lower than that of $CD4^+$
281 T-cells (**Fig. S6B**). Furthermore, $CD8^+$ T-cell tumoricidal activity required neither TNFA (**Fig.**
282 **6SC**) nor degranulation (**Fig. S6D**) and was therefore distinct mechanistically from that of
283 $CD4^+$ T-cells.

284 Thus, we conclude that greatly increased T_H:CTL ratio within tumors treated with *uv*-
285 Reo/sorafenib therapy (**Fig. 2D**) combined with enhanced levels of TNFA, IFNG, IFNB and
286 CCL5, allow efficient control of tumor growth *in vivo* mediated by T_H1-activated $CD4^+$ T-cells,
287 *via* at least two distinct antigen-independent HCC killing mechanisms.

288 **DISCUSSION**

289 This study demonstrates superior efficacy for an immunotherapeutic approach to HCC
290 treatment combining *uv*-inactivated, replication-deficient reovirus with the targeted agent,
291 sorafenib. This combination therapy significantly extended the survival of mice bearing HCC
292 tumors and exerted its anti-tumor activity by engaging a multi-faceted, antigen-independent
293 response from cytotoxic $CD4^+$ T_H-cells (CTHs). Notably, this therapy was superior to when
294 Reo was used in combination, allowing us to map the response *via* differential analysis *in vivo*
295 and *in vitro*.

296

297 The response stems from *uv*-Reo/sorafenib induced expression of both the chemokine, CCL5,
298 as well as IFNB; both are likely induced because of increased IRF3 phosphorylation compared
299 with Reo in combination. Elevated expression of CCL5 led to increased accumulation of
300 $CCR5^+$ T_H1-activated $CD4^+$ T-cells in tumors, thereby skewing the CD4:CD8 T-cell ratio in
301 favor of T_H1-cells, which was not observed with any other treatment. These tumor-infiltrating
302 lymphocytes (TILs) exerted paracrine tumoricidal activity *via* TNFA, the response to which
303 was enhanced in HCC cells by both IFNG and sorafenib. Concomitantly, increased expression
304 of IFNB in HCC cells following stimulation with *uv*-Reo/sorafenib was a crucial mechanistic
305 switch, stimulating an antigen/perforin-independent degranulation mechanism involving
306 GZMB that required close cell-cell contact. Hence, our findings support that *uv*-inactivated
307 reovirus could be used to enhance the efficacy of sorafenib during the treatment of HCC by
308 engaging $TNFA^+GZMB^+PRF^{neg}$ T_H1-cells.

309

310 CCL5 (RANTES) is a C-C motif containing chemokine with a pleiotropic role in cancer
311 biology, being secreted by and acting on both immune and tumor cell compartments. In the
312 latter, CCL5 promotes epithelial-to-mesenchyme transition (EMT) and increases cancer cell

313 motility, thereby driving invasion and metastasis in numerous of cancer types (*46, 47*). In the
314 former, CCL5 recruits a variety of leukocytes, including monocytes, NK cells, and $CD4^+$ T-
315 cells, through binding to one of its cognate receptors, namely CCRs 1, 3 and 5. Reo-induced
316 expression of CCL5 has been demonstrated in numerous cancer models, including melanoma,
317 prostate, and ovarian, both *in vitro* and *in vivo* (*6, 8, 9, 11*). However, here, we showed that
318 CCL5 was more strongly induced in HCCs by *uv*-Reo, not Reo, suggesting that the former was
319 a more potent innate immune stimulant, consistent with the enhanced activation seen in the
320 intracellular signalling pathways of infected HCCs. This differential response was also
321 observed in PBMCs *in vitro*, demonstrating that this phenomenon was not restricted to
322 malignant cells. Consequently, the precise cell type(s) responsible for the expression pattern
323 of CCL5 *in vivo* have yet to be defined, but this likely arises from the combined contributions
324 of a heterogeneous population of cells responding to Reo/*uv*-Reo.
325
326 Activated T_H-cells can develop into a variety of functionally distinct subpopulations each
327 expressing a unique repertoire of chemokine receptors, including those responsive to CCL5.
328 T_H1-cells drive cell-mediated anti-tumor immune responses, produce large amounts of the
329 inflammatory cytokines TNFA and IFNG, and favor CCR5 (*48*). T_H2-cells drive humoral
330 responses, produce large amounts of IL4 and IL13, and favor CCR3 (*48*). Collectively, the
331 results of our cytokine, chemokine, and receptor expression analyses are consistent with the
332 CCL5-driven recruitment of T_H1-cells into tumors undergoing *uv*-Reo/sorafenib therapy.
333 Consequently, in the absence of equivalently increased $CD8^+$ T-cell recruitment, the intra-
334 tumoral CD4:CD8 T-cell ratio is skewed in favor of T_H1-cells.
335
336 TNFA was originally identified because of its ability to induce detectable cytolysis in some
337 tumor cell lines (*49*), including HCC (*50*). However, the role of TNF in liver cancer is complex

338 and studies are often contradictory. There is a considerable body of evidence detailing a pro-
339 tumorigenic role for TNF in the development of liver cancer (*51, 52*) and attempts to exploit
340 TNF as an anti-cancer therapy met with limited success and significant toxicity, when
341 administered systemically as a single agent (*53*). In pre-clinical cancer models, direct intra-
342 tumoral injection of TNF resulted in widespread necrosis. However, much of this effect was
343 attributed to the anti-vascular activity of TNF, rather than direct cytolysis (*54, 55*), as necrosis
344 was absent in avascular tumors (*56*). Therefore, the scientific consensus is that TNF possess
345 weak direct cytolytic activity when administered as a single agent and this is consistent with
346 our findings here in HCC. However, this limited tumoricidal activity can be significantly
347 enhanced by co-administration of IFNG, a phenomenon demonstrated in a variety of tumor
348 types, including melanoma, breast, pancreatic, colon, Ewing's sarcoma, and insulinomas (*54,*
349 *55, 57-60*), confirmed again here in our study on HCC. We now add to this by demonstrating
350 that HCCs are sensitized to TNFA-induced cell death by the targeted TKI sorafenib. Sorafenib
351 is recognized for sensitizing tumor cells to death induced by members of the TNF family,
352 including TRAIL and Fas, a process attributed to the downregulation of the anti-apoptotic
353 protein Mcl-1 (*39, 40*). Although it is likely that the response to TNFA is enhanced by sorafenib
354 in a similar way, the precise mechanism has yet to be determined. Interestingly, we also found
355 that the killing of HCCs by T_H1-cells, mediated by TNFA/IFNG, occurred even in the presence
356 of the pan-caspase inhibitor Z-VAD-FMK, implicating a caspase-independent pathway.
357
358 These data provide an important mechanistic insight and suggest that the efficacy of *uv*-
359 Reo/sorafenib therapy is underpinned, at least in part, by a skewing of T-cell ratios in favor of
360 $IFNG^+$ $TNFA^+$ T_H1-cells. However, their expression of IFNG and TNFA does not fully explain
361 how they control tumor growth in response to *uv*-Reo/sorafenib and not in other treatment
362 groups where they are also equally abundant.

363 We, and others, have demonstrated that *uv*-Reo elicits a significantly more robust induction of
364 IFNB (a type-I interferon) in treated cells compared with Reo (*41, 61*). Here, we have
365 confirmed these findings in both human and murine HCC cells. Our analysis indicates that this
366 differential expression of IFNB could be attributed to the presence of a virulence factor
367 produced by Reo that dampens the innate response to viral infection. Several reoviral proteins
368 have been implicated as suppressors of the interferon response, including the non-structural
369 protein μNS (*42*) and the structural protein σ3 (*43*). It is likely that one or both contribute to
370 the suppression of IFNB in HCCs infected with Reo, but not *uv*-Reo. The pattern of IFNB
371 expression *in vivo* likely reflects the contributions from a heterogeneous collection of cell types
372 *e.g.,* immune, stromal, vascular and cancerous, all growing in 3D.
373
374 This study demonstrates that IFNB induces a GZMB-mediated, antigen/perforin-independent,
375 short-range tumoricidal activity in T_H1-cells. The expression of GZMB by $CD4^+$ T-cells is not
376 typically taught as part of conventional T-cell dogma but is well-documented in the context of
377 viral infection (*22, 26-28, 32, 33*). However, reports of perforin-independent, GZMB-mediated
378 killing mediated by $CD4^+$ T-cells are so infrequent that we could not find examples in the
379 reviewed literature. Hence, this study breaks new ground by demonstrating antigen-
380 independent mechanisms exerting toxicity against HCC. The precise mechanisms through
381 which GZMB mediates cellular toxicity in the absence of perforin remain incompletely
382 understood. Various cell entry pathways have been described, including pinocytosis (*62, 63*)
383 and the binding to surface moieties such as the cation-independent mannose-6-phosphate
384 receptor (CI-MPR) (*64, 65*), heparin sulfate proteoglycans (*65*), and membrane-bound hsp70
385 (*66*). GZMB has also been demonstrated to play an extracellular role, wherein the digestion of
386 extracellular matrix proteins such as vitronectin, fibronectin and laminin induced apoptosis in

387 cells sensitive to anoikis (*67*). However, whether T_H1-derived GZMB exerts its cytotoxic
388 activity against HCC cells *via* intra-cellular or extra-cellular pathways has yet to be determined.
389
390 $CD8^+$ T-cells were also present in tumors treated with *uv*-Reo/sorafenib therapy. Consequently,
391 this study cannot completely exclude the possibility that they contribute, albeit in a minor
392 capacity, to the efficacy of *uv*-Reo/sorafenib therapy. In the context of antigen-independent
393 immunity, $CD8^+$ T-cells were less tumoricidal than their $CD4^+$ counterparts, and utilised
394 mechanisms independent of TNFA and GZMB. The abundance of $CD8^+$ T-cells was also
395 unchanged in *uv*-Reo/sorafenib treated tumors relative to live Reo controls. Consequently, the
396 CD4:CD8 T-cell ratio was significantly skewed in favor of the former, indicating that T_H-cells
397 were likely the dominant immune effector cell type in tumors responding to *uv*-Reo/sorafenib
398 therapy. However, this study cannot discount a role for antigen-specific immunity in the delay
399 of tumor re-growth following the cessation of *uv*-Reo/sorafenib therapy (Post-therapy phase),
400 which also contributed significantly to the therapy-induced overall survival advantage, and this
401 remains the focus of ongoing research.
402
403 Taken together, our data demonstrate an antigen/perforin-independent immune response
404 mediated by $GZMB^+$ T_H1-cells against hepatocellular carcinoma, induced by the unusual
405 combination of *uv*-inactivated reovirus and the targeted agent, sorafenib. This highlights a
406 possibly overlooked role for $GZMB^+CD4^+$ T_H1-cells in mediating antigen-independent anti-
407 tumor immunity, and further work is needed to fully understand how non-canonical effector
408 cells can be exploited as a therapeutic tool for the treatment of HCC.

409 **MATERIALS & METHODS**

410

411 **Mouse models**

412 All *in vivo* experiments were conducted with the approval of the University of Leeds
413 Applications and Amendments (Ethics) Committee and in accordance with UK Home Office
414 regulations (PP1816772). BALB/c mice (BALB/cAnNCrl [Charles River Laboratories]) were
415 housed in individually ventilated cages. SCID (CB17-Prkdc^{SCID} [St. James Biomedical
416 Services]) and SCID/Beige (CB17-Prkdc^{SCID} Lyst^{bg} [Charles River Laboratories]) mice were
417 housed in isolator cages. All mice were housed with 12-h light/dark cycles at 22°C with access
418 to food and water *ad libitum*. For overall survival studies, female mice, aged 7 – 8 weeks, were
419 implanted subcutaneously (*s.c.,*) with 1MEA cells in 100 μL of PBS. Once palpable (~2 – 3
420 mm in diameter), tumor-bearing mice were treated with either live- or *uv*-reo (1x10^{7} pfu)
421 (Oncolytics, Calgary, AB, Canada) in 50 μL of PBS *via* intra-tumoral injection (*i.t.,*), three
422 times per week for six weeks. Reovirus or vehicle (PBS) were given alone or in combination
423 with sorafenib (10 mg/Kg) (Cell Guidance Systems, St. Louis, MO, US) or vehicle (PBS, 25%
424 polyethylene glycol 400, 5% Tween-20, 5% ethanol) *via* oral gavage (*o.g.,*), daily for 4 four
425 weeks. Mice were regularly examined for signs of deterioration in health or weight loss.
426 Tumour diameter was measured in two dimensions using callipers and mice were culled by an
427 approved schedule 1 method when they reached 15 mm in diameter, and this was used as a
428 proxy for predicting cancer-induced mortality. For histological, proteomic and RNA analyses,
429 female mice were implanted with murine HCC cells and treated with live- or *uv*-reo alone or
430 in combination with sorafenib or vehicle as described above, for two weeks. Twenty-four hours
431 after the last treatment the mice were culled by an approved Schedule 1 method and tissue
432 processed accordingly.

433 **Primary cell cultures and cell lines**

434 Human HCC cell line 'HLE" (Japanese Collection of Research Bioresources [JCRB], Japan)
435 and the murine HCC cell line '1ME A7.7R.1' (1MEA) (American Tissue Culture Collection
436 [ATCC], Manassas, VA, US) were cultured at 37ºC in humidified 5% CO_2 in complete growth
437 medium comprising DMEM supplemented with 2 mM *l*-glutamine, 10% fetal bovine serum
438 (FBS), and 1 % non-essential amino acids (NEAA) (Thermo Fisher Scientific, Waltham, MA,
439 US). Primary human T-cells were isolated from peripheral blood (NHS Blood & Transplant
440 Service, UK) using Ficoll-Paque™ (Merck Group, Darmstadt, Germany) density gradient
441 centrifugation followed by positive selection using antibody-coated magnetic beads directed
442 against either human CD4 or CD8 antigen (Miltenyi Biotechnology, Cologne, Germany).
443 Isolated $CD4^+$ T-cells were either maintained in a naïve state by seeding in complete growth
444 medium alone or underwent T_H1-activation in tissue culture flasks pre-coated with anti-human
445 CD3 antibody (10 µg/mL) (BioLegend, San Diego, CA, US) in complete medium
446 supplemented with anti-human CD28 antibody (5 µg/mL) (BioLegend, San Diego, CA, US),
447 rhIL2 (50 U/mL) (BioLegend, San Diego, CA, US) and rhIL12 (10 ng/mL) (Peprotech,
448 Cranbury, NJ, US), for three days. Isolated $CD8^+$ T-cells were kept in a naïve state or activated
449 as described for T_H1-cells, but in the absence of rhIL12.

450

451 Murine $CD4^+$ T-cells were isolated from BALB/c mice using a CD4 negative magnetic
452 selection kit (Miltenyi Biotechnology, Cologne, Germany) on single cell suspensions generated
453 from mouse spleens and lymph nodes. Naïve $CD4^+$ T-cells were seeded into tissue culture
454 flasks, pre-coated with anti-mouse CD3 antibody (3 μg/mL), in complete medium
455 supplemented with anti-mouse CD28 antibody (3 μg/mL), anti-mouse IL4 (10 μg/mL) and
456 recombinant mouse IL2 (5 ng/mL) and IL12 (10 ng/mL) (BioLegend, San Diego, CA, US), for
457 three days prior to use.

458 **Chemotaxis assay**

459 Naïve or T_H1-activated $CD4^+$ T-cells were serum-starved for two hours in chemotaxis buffer
460 comprising RPMI-1640 (Thermo Fisher Scientific, Waltham, MA, US) and 0.5% BSA (Merck
461 Group, Darmstadt, Germany) before use. For each assay, $3x10^5$ naïve or T_H1-activated $CD4^+$
462 T-cells were labelled with CFSE and seeded into tissue culture inserts (5 μm pore size), in 24-
463 well plates, in chemotaxis buffer (RPMI-1640 + 0.5% BSA) with or without the CCR5 inhibitor
464 (Maraviroc, 1 μM) or vehicle. The lower compartment contained either chemotaxis buffer
465 alone or was supplemented with rhCCL5 (100 ng/mL) with or without Maraviroc or vehicle.
466 Chemotaxis was allowed to proceed for 1.5 hours prior to cell counting using a CytoFLEX S
467 flow cytometer.

468

469 **Immunofluorescence**

470 Tumor cryosections 14 μm thick were fixed with either ice-cold acetone (3 – 5 mins) or 4%
471 paraformaldehyde (PFA) (5 mins) with permeabilization using 0.1% Triton-X100 (5 mins).
472 Fixed sections were blocked with goat serum (10%) (Thermo Fisher Scientific, Waltham, MA,
473 US) for 1 hour and incubated with fluorophore-conjugated primary antibodies (2 – 5 μg/mL)
474 overnight at 4°C. Nuclei were counter-stained using DAPI (Thermo Fisher Scientific, Waltham,
475 MA, US) and labelled sections were mounted in ProLong Diamond antifade reagent (Thermo
476 Fisher Scientific, Waltham, MA, US). Images of random fields of view (F.O.V.) were acquired
477 using both Nikon A1R (Nikon, Tokyo, Japan) and Zeiss LSM 980 (Zeiss Group, Oberkochen,
478 Germany) confocal microscopes. Image processing and quantification was performed using
479 'Fiji' Image J (National Institutes of Health [NIH], Bethesda, MD, US).

480 **Proteomics**

481 For cytokine array, tumor protein extracts were generated from snap-frozen biopsies using a
482 combination of TissueLyser LT (Qiagen, Hilden, Germany) and four rounds of freeze/thaw
483 cycling, in PBS. Mouse cytokine arrays (Cytokine array 'C3' [Raybiotech, Peachtree Corners,
484 GA, US]) were incubated with 1 mg total protein pooled from samples in the indicated
485 treatment groups, taking an equal amount of protein from each sample. Membranes were
486 developed using chemiluminescent substrate with a ChemiDoc™ imaging system (Bio
487 Laboratories, Hercules, CA, US) and image quantification was performed using 'Fiji' Image J.
488 For ELISAs, debris-cleared supernatants were collected from human and mouse HCC cell lines
489 following overnight incubation with live/*uv*-reo (2 PFU/cell) and from T-cells at three days
490 post-activation. ELISAs were performed against human and mouse IFNB and CCL5, and
491 human TNFA, IFNG and TRAIL as described in the manufacturer's instructions.

492

493 **Flow cytometry**

494 HCC cell lines were detached, and T-cells were pelleted, then washed twice in HBSS (Thermo
495 Fisher Scientific, Waltham, MA, US) and resuspended in staining buffer (HBSS + 0.5% BSA),
496 on ice. Directly-conjugated antibodies (2 – 5 μg/mL) were incubated with cells for 30-minutes
497 on ice and the labelled cells were then washed twice with ice-cold staining buffer prior to
498 analysis. For tumour specimens, biopsies preserved in 90% FCS and 10% DMSO were thawed
499 at 37°C in a water bath, wash twice in ice-cold HBSS and forced through a 70 μm nylon mesh
500 using a syringe insert. Single cell suspensions were labelled with antibodies against cell surface
501 antigens as described above and then prepared using a Cyto-Fast Fix/Perm kit (BioLegend, San
502 Diego, CA, US), according to the manufacturer's instructions, prior to staining of intra-cellular
503 antigens on ice for 30-minutes in Perm buffer. Fully stained cells were washed twice each in

504 Perm buffer and staining buffer prior to data collection. Data were collected using a CytoFLEX
505 S flow cytometer and analysed using FlowJo software (FlowJo Llc, Ashland, OR, US).

506 **HCC/T-cell co-culture assays**

507 For standard target cell killing assays, human and murine HCC cells were labelled with
508 carboxyfluorescein succinimidyl ester (CFSE) (Thermo Fisher Scientific, Waltham, MA, US),
509 seeded into 96-well plates (1.5 x10^4 cells/well) and allowed to attach overnight. Naïve and
510 T_H1-activated $CD4^+$ T-cells were labelled with near infra-red dye (NIR) (Thermo Fisher
511 Scientific, Waltham, MA, US) and seeded with target HCC cells at a ratio of 50:1 (E:T ratio)
512 in the presence or absence of rIFNB (500 ng/mL human [Peprotech, Cranbury, NJ, US]; 50
513 ng/mL murine [BioLegend, San Diego, CA, US]), with or without neutralizing antibodies or
514 EGTA, where indicated. Following overnight incubation, all cells were collected, including
515 adherent and non-adherent, then labelled with Zombie UV viability dye (BioLegend, San
516 Diego, CA, US), and fixed in 4% PFA prior to analysis. Target cell killing was determined
517 using a CytoFLEX S flow cytometer. For assays involving tissue culture inserts, target HCCs
518 were labelled as described above and seeded into 24-well plates (3.0 x10^4 cells/well). NIR-
519 labelled $CD4^+$ T-cells were seeded into the upper chamber of a tissue culture insert (0.4 μm
520 pore size) and rIFNB was added to both upper and lower compartments, simultaneously.
521 Following overnight incubation, adherent and non-adherent cells were collected for analysis
522 from the lower compartment only.

523

524 **Statistics**

525 All figures and statistical analyses were performed using Prism software (GraphPad, San
526 Diego, CA). All data presented are expressed as means ± standard error of the mean (SEM)
527 and were analysed by one-tailed or two-tailed unpaired Student's t-test where appropriate. P

528 values less than 0.05 were considered statistically significant. Sample size (n) is indicated
529 where appropriate in figure legends.

530 **List of Supplementary Materials**

531 Fig. S1 – S6, supplementary figures and legends.

532 **References and Notes**

533 1. D. Kitagawa, K. Yokota, M. Gouda, Y. Narumi, H. Ohmoto, E. Nishiwaki, K. Akita, Y.
534 Kirii, Activity-based kinase profiling of approved tyrosine kinase inhibitors. *Genes Cells*
535 **18**, 110-122 (2013).

536 2. R. V. Iyer, O. Maguire, M. Kim, L. I. Curtin, S. Sexton, D. T. Fisher, S. A. Schihl, G.
537 Fetterly, S. Menne, H. Minderman, Dose-Dependent Sorafenib-Induced
538 Immunosuppression Is Associated with Aberrant NFAT Activation and Expression of
539 PD-1 in T Cells. *Cancers (Basel)* **11**, (2019).

540 3. W. Zhao, Y. H. Gu, R. Song, B. Q. Qu, Q. Xu, Sorafenib inhibits activation of human
541 peripheral blood T cells by targeting LCK phosphorylation. *Leukemia* **22**, 1226-1233
542 (2008).

543 4. J. M. Llovet, S. Ricci, V. Mazzaferro, P. Hilgard, E. Gane, J. F. Blanc, A. C. de Oliveira,
544 A. Santoro, J. L. Raoul, A. Forner, M. Schwartz, C. Porta, S. Zeuzem, L. Bolondi, T. F.
545 Greten, P. R. Galle, J. F. Seitz, I. Borbath, D. Haussinger, T. Giannaris, M. Shan, M.
546 Moscovici, D. Voliotis, J. Bruix, S. I. S. Group, Sorafenib in advanced hepatocellular
547 carcinoma. *N Engl J Med* **359**, 378-390 (2008).

548 5. V. Bernstein, S. L. Ellard, S. F. Dent, D. Tu, M. Mates, S. K. Dhesy-Thind, L. Panasci,
549 K. A. Gelmon, M. Salim, X. Song, M. Clemons, D. Ksienski, S. Verma, C. Simmons, H.
550 Lui, K. Chi, H. Feilotter, L. J. Hagerman, L. Seymour, A randomized phase II study of
551 weekly paclitaxel with or without pelareorep in patients with metastatic breast cancer:
552 final analysis of Canadian Cancer Trials Group IND.213. *Breast Cancer Res Treat* **167**,
553 485-493 (2018).

554 6. D. R. Clements, A. M. Sterea, Y. Kim, E. Helson, C. A. Dean, A. Nunokawa, K. M.
555 Coyle, T. Sharif, P. Marcato, S. A. Gujar, P. W. Lee, Newly recruited CD11b+, GR-1+,
556 Ly6C(high) myeloid cells augment tumor-associated immunosuppression immediately
557 following the therapeutic administration of oncolytic reovirus. *J Immunol* **194**, 4397-
558 4412 (2015).

559 7. F. Errington, L. Steele, R. Prestwich, K. J. Harrington, H. S. Pandha, L. Vidal, J. de
560 Bono, P. Selby, M. Coffey, R. Vile, A. Melcher, Reovirus activates human dendritic cells
561 to promote innate antitumor immunity. *J Immunol* **180**, 6018-6026 (2008).

562 8. F. Errington, C. L. White, K. R. Twigger, A. Rose, K. Scott, L. Steele, L. J. Ilett, R.
563 Prestwich, H. S. Pandha, M. Coffey, P. Selby, R. Vile, K. J. Harrington, A. A. Melcher,
564 Inflammatory tumour cell killing by oncolytic reovirus for the treatment of melanoma.
565 *Gene Ther* **15**, 1257-1270 (2008).

566 9. S. A. Gujar, P. Marcato, D. Pan, P. W. Lee, Reovirus virotherapy overrides tumor
567 antigen presentation evasion and promotes protective antitumor immunity. *Mol Cancer*
568 *Ther* **9**, 2924-2933 (2010).

569 10. R. J. Prestwich, F. Errington, E. J. Ilett, R. S. Morgan, K. J. Scott, T. Kottke, J.
570 Thompson, E. E. Morrison, K. J. Harrington, H. S. Pandha, P. J. Selby, R. G. Vile, A.
571 A. Melcher, Tumor infection by oncolytic reovirus primes adaptive antitumor immunity.
572 *Clin Cancer Res* **14**, 7358-7366 (2008).

573 11. R. J. Prestwich, F. Errington, L. P. Steele, E. J. Ilett, R. S. Morgan, K. J. Harrington, H.
574 S. Pandha, P. J. Selby, R. G. Vile, A. A. Melcher, Reciprocal human dendritic cell-
575 natural killer cell interactions induce antitumor activity following tumor cell infection by
576 oncolytic reovirus. *J Immunol* **183**, 4312-4321 (2009).

577 12. R. J. Prestwich, E. J. Ilett, F. Errington, R. M. Diaz, L. P. Steele, T. Kottke, J. Thompson,
578 F. Galivo, K. J. Harrington, H. S. Pandha, P. J. Selby, R. G. Vile, A. A. Melcher, Immune-
579 mediated antitumor activity of reovirus is required for therapy and is independent of
580 direct viral oncolysis and replication. *Clin Cancer Res* **15**, 4374-4381 (2009).

581 13. K. Rajani, C. Parrish, T. Kottke, J. Thompson, S. Zaidi, L. Ilett, K. G. Shim, R. M. Diaz,
582 H. Pandha, K. Harrington, M. Coffey, A. Melcher, R. Vile, Combination Therapy With
583 Reovirus and Anti-PD-1 Blockade Controls Tumor Growth Through Innate and
584 Adaptive Immune Responses. *Mol Ther* **24**, 166-174 (2016).

585 14. C. L. White, K. R. Twigger, L. Vidal, J. S. De Bono, M. Coffey, L. Heinemann, R.
586 Morgan, A. Merrick, F. Errington, R. G. Vile, A. A. Melcher, H. S. Pandha, K. J.
587 Harrington, Characterization of the adaptive and innate immune response to
588 intravenous oncolytic reovirus (Dearing type 3) during a phase I clinical trial. *Gene Ther*
589 **15**, 911-920 (2008).

590 15. D. Mahalingam, S. Goel, S. Aparo, S. Patel Arora, N. Noronha, H. Tran, R.
591 Chakrabarty, G. Selvaggi, A. Gutierrez, M. Coffey, S. T. Nawrocki, G. Nuovo, M. M.
592 Mita, A Phase II Study of Pelareorep (REOLYSIN((R))) in Combination with
593 Gemcitabine for Patients with Advanced Pancreatic Adenocarcinoma. *Cancers (Basel)*
594 **10**, (2018).

595 16. E. Galanis, S. N. Markovic, V. J. Suman, G. J. Nuovo, R. G. Vile, T. J. Kottke, W. K.
596 Nevala, M. A. Thompson, J. E. Lewis, K. M. Rumilla, V. Roulstone, K. Harrington, G.
597 P. Linette, W. J. Maples, M. Coffey, J. Zwiebel, K. Kendra, Phase II trial of intravenous
598 administration of Reolysin((R)) (Reovirus Serotype-3-dearing Strain) in patients with
599 metastatic melanoma. *Mol Ther* **20**, 1998-2003 (2012).

600 17. R. Gollamudi, M. H. Ghalib, K. K. Desai, I. Chaudhary, B. Wong, M. Einstein, M. Coffey,
601 G. M. Gill, K. Mettinger, J. M. Mariadason, S. Mani, S. Goel, Intravenous administration
602 of Reolysin, a live replication competent RNA virus is safe in patients with advanced
603 solid tumors. *Invest New Drugs* **28**, 641-649 (2010).

604 18. A. M. Noonan, M. R. Farren, S. M. Geyer, Y. Huang, S. Tahiri, D. Ahn, S. Mikhail, K. K.
605 Ciombor, S. Pant, S. Aparo, J. Sexton, J. L. Marshall, T. A. Mace, C. S. Wu, B. El-
606 Rayes, C. D. Timmers, J. Zwiebel, G. B. Lesinski, M. A. Villalona-Calero, T. S. Bekaii-
607 Saab, Randomized Phase 2 Trial of the Oncolytic Virus Pelareorep (Reolysin) in
608 Upfront Treatment of Metastatic Pancreatic Adenocarcinoma. *Mol Ther* **24**, 1150-1158
609 (2016).

610 19. D. W. Sborov, G. J. Nuovo, A. Stiff, T. Mace, G. B. Lesinski, D. M. Benson, Jr., Y. A.
611 Efebera, A. E. Rosko, F. Pichiorri, M. R. Grever, C. C. Hofmeister, A phase I trial of
612 single-agent reolysin in patients with relapsed multiple myeloma. *Clin Cancer Res* **20**,
613 5946-5955 (2014).

614 20. L. Vidal, H. S. Pandha, T. A. Yap, C. L. White, K. Twigger, R. G. Vile, A. Melcher, M.
615 Coffey, K. J. Harrington, J. S. DeBono, A phase I study of intravenous oncolytic reovirus
616 type 3 Dearing in patients with advanced cancer. *Clin Cancer Res* **14**, 7127-7137
617 (2008).

618 21. D. Mahalingam, G. A. Wilkinson, K. H. Eng, P. Fields, P. Raber, J. L. Moseley, K.
619 Cheetham, M. Coffey, G. Nuovo, P. Kalinski, B. Zhang, S. P. Arora, C. Fountzilas,
620 Pembrolizumab in Combination with the Oncolytic Virus Pelareorep and
621 Chemotherapy in Patients with Advanced Pancreatic Adenocarcinoma: A Phase Ib
622 Study. *Clin Cancer Res* **26**, 71-81 (2020).

623 22. A. Saez-Borderias, M. Guma, A. Angulo, B. Bellosillo, D. Pende, M. Lopez-Botet,
624 Expression and function of NKG2D in CD4+ T cells specific for human
625 cytomegalovirus. *Eur J Immunol* **36**, 3198-3206 (2006).

626 23. M. A. Suni, S. A. Ghanekar, D. W. Houck, H. T. Maecker, S. B. Wormsley, L. J. Picker,
627 R. B. Moss, V. C. Maino, CD4(+)CD8(dim) T lymphocytes exhibit enhanced cytokine
628 expression, proliferation and cytotoxic activity in response to HCMV and HIV-1
629 antigens. *Eur J Immunol* **31**, 2512-2520 (2001).

630 24. E. M. van Leeuwen, E. B. Remmerswaal, M. T. Vossen, A. T. Rowshani, P. M.
631 Wertheim-van Dillen, R. A. van Lier, I. J. ten Berge, Emergence of a CD4+CD28-
632 granzyme B+, cytomegalovirus-specific T cell subset after recovery of primary
633 cytomegalovirus infection. *J Immunol* **173**, 1834-1841 (2004).

634 25. J. J. Zaunders, W. B. Dyer, B. Wang, M. L. Munier, M. Miranda-Saksena, R. Newton,
635 J. Moore, C. R. Mackay, D. A. Cooper, N. K. Saksena, A. D. Kelleher, Identification of
636 circulating antigen-specific CD4+ T lymphocytes with a CCR5+, cytotoxic phenotype
637 in an HIV-1 long-term nonprogressor and in CMV infection. *Blood* **103**, 2238-2247
638 (2004).

639 26. N. Aslan, C. Yurdaydin, J. Wiegand, T. Greten, A. Ciner, M. F. Meyer, H. Heiken, B.
640 Kuhlmann, T. Kaiser, H. Bozkaya, H. L. Tillmann, A. M. Bozdayi, M. P. Manns, H.
641 Wedemeyer, Cytotoxic CD4 T cells in viral hepatitis. *J Viral Hepat* **13**, 505-514 (2006).

642 27. P. J. Norris, H. F. Moffett, O. O. Yang, D. E. Kaufmann, M. J. Clark, M. M. Addo, E. S.
643 Rosenberg, Beyond help: direct effector functions of human immunodeficiency virus
644 type 1-specific CD4(+) T cells. *J Virol* **78**, 8844-8851 (2004).

645 28. D. Adhikary, U. Behrends, A. Moosmann, K. Witter, G. W. Bornkamm, J. Mautner,
646 Control of Epstein-Barr virus infection in vitro by T helper cells specific for virion
647 glycoproteins. *J Exp Med* **203**, 995-1006 (2006).

648 29. R. Khanna, S. R. Burrows, P. M. Steigerwald-Mullen, D. J. Moss, M. G. Kurilla, L.
649 Cooper, Targeting Epstein-Barr virus nuclear antigen 1 (EBNA1) through the class II
650 pathway restores immune recognition by EBNA1-specific cytotoxic T lymphocytes:
651 evidence for HLA-DM-independent processing. *Int Immunol* **9**, 1537-1543 (1997).

652 30. E. Landais, X. Saulquin, E. Scotet, L. Trautmann, M. A. Peyrat, J. L. Yates, W. W.
653 Kwok, M. Bonneville, E. Houssaint, Direct killing of Epstein-Barr virus (EBV)-infected
654 B cells by CD4 T cells directed against the EBV lytic protein BHRF1. *Blood* **103**, 1408-
655 1416 (2004).

656 31. H. M. Long, T. A. Haigh, N. H. Gudgeon, A. M. Leen, C. W. Tsang, J. Brooks, E.
657 Landais, E. Houssaint, S. P. Lee, A. B. Rickinson, G. S. Taylor, CD4+ T-cell responses
658 to Epstein-Barr virus (EBV) latent-cycle antigens and the recognition of EBV-
659 transformed lymphoblastoid cell lines. *J Virol* **79**, 4896-4907 (2005).

660 32. E. R. Jellison, S. K. Kim, R. M. Welsh, Cutting edge: MHC class II-restricted killing in
661 vivo during viral infection. *J Immunol* **174**, 614-618 (2005).

662 33. K. A. Stuller, E. Flano, CD4 T cells mediate killing during persistent gammaherpesvirus
663 68 infection. *J Virol* **83**, 4700-4703 (2009).

664 34. T. Brunner, R. J. Mogil, D. LaFace, N. J. Yoo, A. Mahboubi, F. Echeverri, S. J. Martin,
665 W. R. Force, D. H. Lynch, C. F. Ware, et al., Cell-autonomous Fas (CD95)/Fas-ligand

666 interaction mediates activation-induced apoptosis in T-cell hybridomas. *Nature* **373**,
667 441-444 (1995).

668 35. A. K. Simon, O. Williams, J. Mongkolsapaya, B. Jin, X. N. Xu, H. Walczak, G. R.
669 Screaton, Tumor necrosis factor-related apoptosis-inducing ligand in T cell
670 development: sensitivity of human thymocytes. *Proc Natl Acad Sci U S A* **98**, 5158-
671 5163 (2001).

672 36. H. Walczak, R. E. Miller, K. Ariail, B. Gliniak, T. S. Griffith, M. Kubin, W. Chin, J. Jones,
673 A. Woodward, T. Le, C. Smith, P. Smolak, R. G. Goodwin, C. T. Rauch, J. C. Schuh,
674 D. H. Lynch, Tumoricidal activity of tumor necrosis factor-related apoptosis-inducing
675 ligand in vivo. *Nat Med* **5**, 157-163 (1999).

676 37. K. M. Detjen, K. Farwig, M. Welzel, B. Wiedenmann, S. Rosewicz, Interferon gamma
677 inhibits growth of human pancreatic carcinoma cells via caspase-1 dependent
678 induction of apoptosis. *Gut* **49**, 251-262 (2001).

679 38. S. Rakshit, B. S. Chandrasekar, B. Saha, E. S. Victor, S. Majumdar, D. Nandi,
680 Interferon-gamma induced cell death: Regulation and contributions of nitric oxide, cJun
681 N-terminal kinase, reactive oxygen species and peroxynitrite. *Biochim Biophys Acta*
682 **1843**, 2645-2661 (2014).

683 39. K. F. Chen, W. T. Tai, T. H. Liu, H. P. Huang, Y. C. Lin, C. W. Shiau, P. K. Li, P. J. Chen,
684 A. L. Cheng, Sorafenib overcomes TRAIL resistance of hepatocellular carcinoma cells
685 through the inhibition of STAT3. *Clin Cancer Res* **16**, 5189-5199 (2010).

686 40. D. Llobet, N. Eritja, A. Yeramian, J. Pallares, A. Sorolla, M. Domingo, M. Santacana, F.
687 J. Gonzalez-Tallada, X. Matias-Guiu, X. Dolcet, The multikinase inhibitor Sorafenib

688 induces apoptosis and sensitises endometrial cancer cells to TRAIL by different
689 mechanisms. *Eur J Cancer* **46**, 836-850 (2010).

690 41. A. Samson, M. J. Bentham, K. Scott, G. Nuovo, A. Bloy, E. Appleton, R. A. Adair, R.
691 Dave, A. Peckham-Cooper, G. Toogood, S. Nagamori, M. Coffey, R. Vile, K. Harrington,
692 P. Selby, F. Errington-Mais, A. Melcher, S. Griffin, Oncolytic reovirus as a combined
693 antiviral and anti-tumour agent for the treatment of liver cancer. *Gut* **67**, 562-573
694 (2018).

695 42. M. L. Stanifer, C. Kischnick, A. Rippert, D. Albrecht, S. Boulant, Reovirus inhibits
696 interferon production by sequestering IRF3 into viral factories. *Sci Rep* **7**, 10873
697 (2017).

698 43. F. Imani, B. L. Jacobs, Inhibitory activity for the interferon-induced protein kinase is
699 associated with the reovirus serotype 1 sigma 3 protein. *Proc Natl Acad Sci U S A* **85**,
700 7887-7891 (1988).

701 44. D. Y. Oh, S. S. Kwek, S. S. Raju, T. Li, E. McCarthy, E. Chow, D. Aran, A. Ilano, C. S.
702 Pai, C. Rancan, K. Allaire, A. Burra, Y. Sun, M. H. Spitzer, S. Mangul, S. Porten, M. V.
703 Meng, T. W. Friedlander, C. J. Ye, L. Fong, Intratumoral CD4(+) T Cells Mediate Anti-
704 tumor Cytotoxicity in Human Bladder Cancer. *Cell* **181**, 1612-1625 e1613 (2020).

705 45. Y. Xie, A. Akpinarli, C. Maris, E. L. Hipkiss, M. Lane, E. K. Kwon, P. Muranski, N. P.
706 Restifo, P. A. Antony, Naive tumor-specific CD4(+) T cells differentiated in vivo
707 eradicate established melanoma. *J Exp Med* **207**, 651-667 (2010).

708 46. T. Kato, Y. Fujita, K. Nakane, K. Mizutani, R. Terazawa, H. Ehara, Y. Kanimoto, T.
709 Kojima, Y. Nozawa, T. Deguchi, M. Ito, CCR1/CCL5 interaction promotes invasion of

710 taxane-resistant PC3 prostate cancer cells by increasing secretion of MMPs 2/9 and
711 by activating ERK and Rac signaling. *Cytokine* **64**, 251-257 (2013).

712 47. T. T. Murooka, R. Rahbar, E. N. Fish, CCL5 promotes proliferation of MCF-7 cells
713 through mTOR-dependent mRNA translation. *Biochem Biophys Res Commun* **387**,
714 381-386 (2009).

715 48. P. Loetscher, M. Uguccioni, L. Bordoli, M. Baggiolini, B. Moser, C. Chizzolini, J. M.
716 Dayer, CCR5 is characteristic of Th1 lymphocytes. *Nature* **391**, 344-345 (1998).

717 49. E. A. Carswell, L. J. Old, R. L. Kassel, S. Green, N. Fiore, B. Williamson, An endotoxin-
718 induced serum factor that causes necrosis of tumors. *Proc Natl Acad Sci U S A* **72**,
719 3666-3670 (1975).

720 50. J. Zhu, M. Jin, J. Wang, H. Zhang, Y. Wu, D. Li, X. Ji, H. Yang, C. Yin, T. Ren, J. Xing,
721 TNFalpha induces Ca(2+) influx to accelerate extrinsic apoptosis in hepatocellular
722 carcinoma cells. *J Exp Clin Cancer Res* **37**, 43 (2018).

723 51. Y. Jing, K. Sun, W. Liu, D. Sheng, S. Zhao, L. Gao, L. Wei, Tumor necrosis factor-alpha
724 promotes hepatocellular carcinogenesis through the activation of hepatic progenitor
725 cells. *Cancer Lett* **434**, 22-32 (2018).

726 52. E. J. Park, J. H. Lee, G. Y. Yu, G. He, S. R. Ali, R. G. Holzer, C. H. Osterreicher, H.
727 Takahashi, M. Karin, Dietary and genetic obesity promote liver inflammation and
728 tumorigenesis by enhancing IL-6 and TNF expression. *Cell* **140**, 197-208 (2010).

729 53. N. J. Roberts, S. Zhou, L. A. Diaz, Jr., M. Holdhoff, Systemic use of tumor necrosis
730 factor alpha as an anticancer agent. *Oncotarget* **2**, 739-751 (2011).

731 54. F. R. Balkwill, A. Lee, G. Aldam, E. Moodie, J. A. Thomas, J. Tavernier, W. Fiers, Human
732 tumor xenografts treated with recombinant human tumor necrosis factor alone or in
733 combination with interferons. *Cancer Res* **46**, 3990-3993 (1986).

734 55. P. G. Brouckaert, G. G. Leroux-Roels, Y. Guisez, J. Tavernier, W. Fiers, In vivo anti-
735 tumour activity of recombinant human and murine TNF, alone and in combination with
736 murine IFN-gamma, on a syngeneic murine melanoma. *Int J Cancer* **38**, 763-769
737 (1986).

738 56. A. Mantovani, E. Dejana, Cytokines as communication signals between leukocytes
739 and endothelial cells. *Immunol Today* **10**, 370-375 (1989).

740 57. A. Abadie, J. Wietzerbin, Involvement of TNF-related apoptosis-inducing ligand
741 (TRAIL) induction in interferon gamma-mediated apoptosis in Ewing tumor cells. *Ann*
742 *N Y Acad Sci* **1010**, 117-120 (2003).

743 58. H. S. Kim, S. Kim, M. S. Lee, IFN-gamma sensitizes MIN6N8 insulinoma cells to TNF-
744 alpha-induced apoptosis by inhibiting NF-kappaB-mediated XIAP upregulation.
745 *Biochem Biophys Res Commun* **336**, 847-853 (2005).

746 59. M. Kimura, M. Haisa, H. Uetsuka, M. Takaoka, T. Ohkawa, R. Kawashima, T.
747 Yamatsuji, M. Gunduz, Y. Kaneda, N. Tanaka, Y. Naomoto, TNF combined with IFN-
748 alpha accelerates NF-kappaB-mediated apoptosis through enhancement of Fas
749 expression in colon cancer cells. *Cell Death Differ* **10**, 718-728 (2003).

750 60. W. H. Schmiegel, J. Caesar, H. Kalthoff, H. Greten, H. W. Schreiber, H. G. Thiele,
751 Antiproliferative effects exerted by recombinant human tumor necrosis factor-alpha

752 (TNF-alpha) and interferon-gamma (IFN-gamma) on human pancreatic tumor cell
753 lines. *Pancreas* **3**, 180-188 (1988).

754 61. D. R. Henderson, W. K. Joklik, The mechanism of interferon induction by UV-irradiated
755 reovirus. *Virology* **91**, 389-406 (1978).

756 62. C. H. Bird, J. Sun, K. Ung, D. Karambalis, J. C. Whisstock, J. A. Trapani, P. I. Bird,
757 Cationic sites on granzyme B contribute to cytotoxicity by promoting its uptake into
758 target cells. *Mol Cell Biol* **25**, 7854-7867 (2005).

759 63. J. A. Trapani, V. R. Sutton, K. Y. Thia, Y. Q. Li, C. J. Froelich, D. A. Jans, M. S. Sandrin,
760 K. A. Browne, A clathrin/dynamin- and mannose-6-phosphate receptor-independent
761 pathway for granzyme B-induced cell death. *J Cell Biol* **160**, 223-233 (2003).

762 64. B. Motyka, G. Korbutt, M. J. Pinkoski, J. A. Heibein, A. Caputo, M. Hobman, M. Barry,
763 I. Shostak, T. Sawchuk, C. F. Holmes, J. Gauldie, R. C. Bleackley, Mannose 6-
764 phosphate/insulin-like growth factor II receptor is a death receptor for granzyme B
765 during cytotoxic T cell-induced apoptosis. *Cell* **103**, 491-500 (2000).

766 65. K. Veugelers, B. Motyka, I. S. Goping, I. Shostak, T. Sawchuk, R. C. Bleackley,
767 Granule-mediated killing by granzyme B and perforin requires a mannose 6-phosphate
768 receptor and is augmented by cell surface heparan sulfate. *Mol Biol Cell* **17**, 623-633
769 (2006).

770 66. C. Gross, W. Koelch, A. DeMaio, N. Arispe, G. Multhoff, Cell surface-bound heat shock
771 protein 70 (Hsp70) mediates perforin-independent apoptosis by specific binding and
772 uptake of granzyme B. *J Biol Chem* **278**, 41173-41181 (2003).

773 67. M. S. Buzza, L. Zamurs, J. Sun, C. H. Bird, A. I. Smith, J. A. Trapani, C. J. Froelich, E.
774 C. Nice, P. I. Bird, Extracellular matrix remodeling by human granzyme B via cleavage
775 of vitronectin, fibronectin, and laminin. *J Biol Chem* **280**, 23549-23558 (2005).

776 **Acknowledgments:**

777 *Funding*: The authors thank the Medical Research Council (Award No: MR/T016205, awarded
778 to SG), and Cancer Research UK (Award No: 29039, awarded to AS) for funding this research,
779 the NHS Blood and Transplant Service for the provision of donor blood samples, the St.
780 James's Biological Services Unit (SBS) for their support with animal welfare and husbandry,
781 and Oncolytics Biotech Inc. for supplying the human *Orthoreovirus*, type-3 Dearing strain.
782 *Author contributions*: Conceptualization, R.H., S.G, A.S., A.M[2]., and A.M[3]; Methodology,
783 R.H., A.M[1]., and S.G; Investigation, R.H., A.S., K.J.S., E.A., M.B., and A.M[1]; Writing –
784 Original, R.H. and S.G; Writing – Review & Editing, R.H., A.S., A.M[1]., A.M[2]., A.M[3]., E.A.,
785 K.J.S., M.B., and S.G; Funding Acquisition, A.S., A.M[2], A.M[3]., E.I., and S.G. *Competing*
786 *Interests*: The authors declare that there are no conflicts of interest. *Data and materials*
787 *availability:* Further information and requests for resources and reagents should be directed to
788 and will be fulfilled by the lead contact, Stephen Griffin. This study did not generate new
789 unique reagents or standardized datasets and does not report the use or original code.

Figure 1

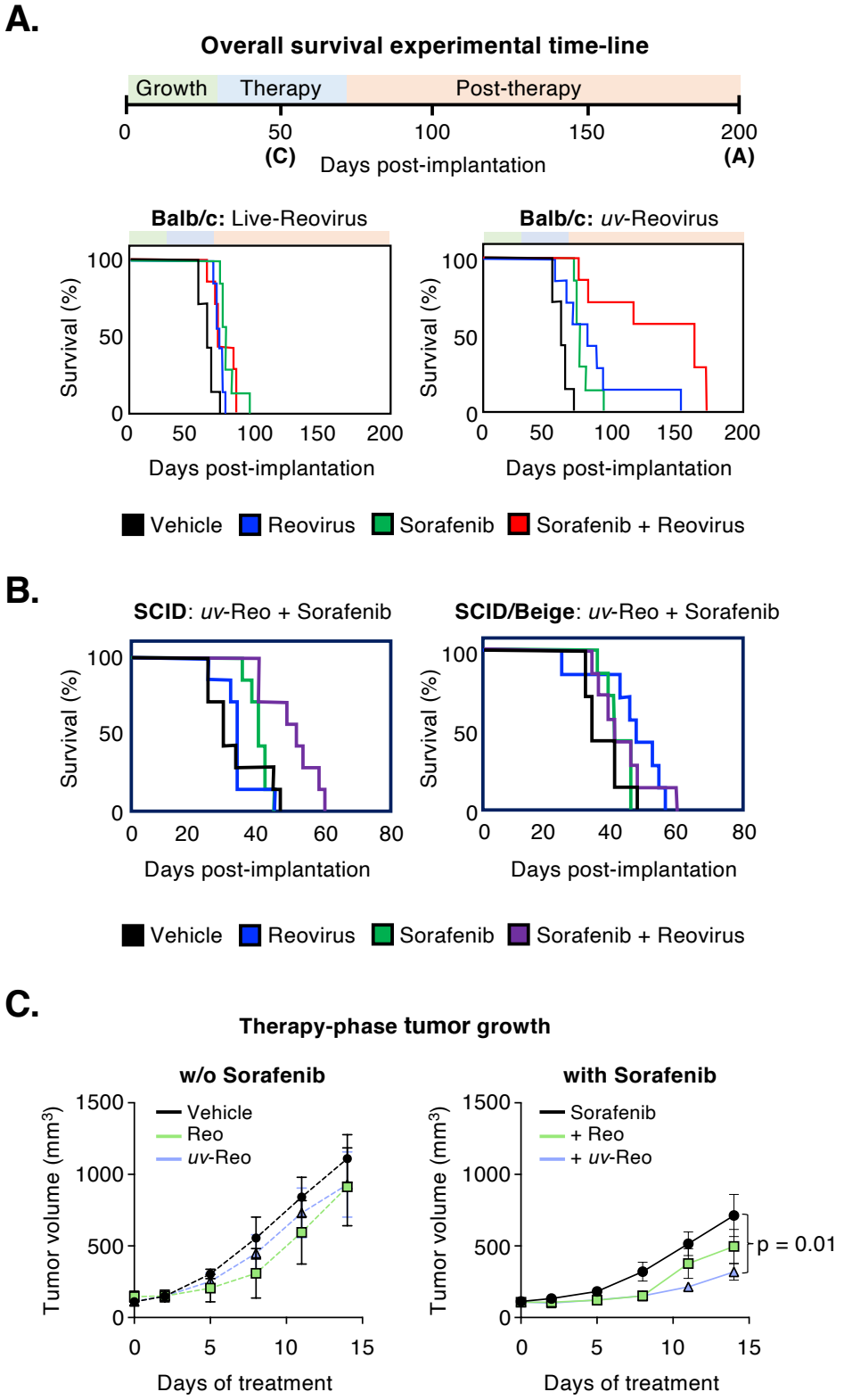
A.
Overall survival experimental time-line
Growth
Therapy
Post-therapy
0
50
100
150
200
(C)
(A)
Days post-implantation
Balb/c: Live-Reovirus
Balb/c: uv-Reovirus
Survival (%)
Days post-implantation
Vehicle
Reovirus
Sorafenib
Sorafenib + Reovirus
B.
SCID: uv-Reo + Sorafenib
SCID/Beige: uv-Reo + Sorafenib
Survival (%)
Days post-implantation
Vehicle
Reovirus
Sorafenib
Sorafenib + Reovirus
C.
Therapy-phase tumor growth
w/o Sorafenib
with Sorafenib
Tumor volume (mm3)
Vehicle
Reo
uv-Reo
Sorafenib
+ Reo
+ uv-Reo
p = 0.01
Days of treatment

Figure 1. The survival of mice bearing syngeneic hepatocellular carcinomas is significantly extended by an immune-mediated mechanism induced by a combination of sorafenib and *uv*-Reo. (**A**) Immunocompetent Balb/c mice bearing HCC tumors were treated with either Reo (*left*) or *uv*-Reo (*right*) alone ($1x10^7$ pfu) or in combination with sorafenib (10 mg/Kg) and tumor volume was monitored over time as a surrogate for cancer-induced mortality (Overall Survival – OS), see experimental design displayed (*top*). Treatments are all significant w.r.t. vehicle ($p \leq 0.05$) and *uv*-Reo+sorafenib was significant w.r.t. *uv*-Reo alone ($p=0.0189$) and sorafenib alone ($p=0.0027$). (**B**) Immunodeficient SCID (*left*) or SCID/Beige (*right*) mice bearing HCC tumors were treated with *uv*-Reo or in combination with sorafenib and overall survival monitored as described above. Treatment with *uv*-Reo+sorafenib was significant w.r.t. all groups in SCID mice only ($p \leq 0.01$). (**C**) Immunocompetent Balb/c mice bearing HCC tumors treated as described in 'A' but culled at two weeks of treatment during the "Therapy-phase" for subsequent analysis, when inhibition of tumor growth was observed (n = 5 mice per condition).

Figure 2

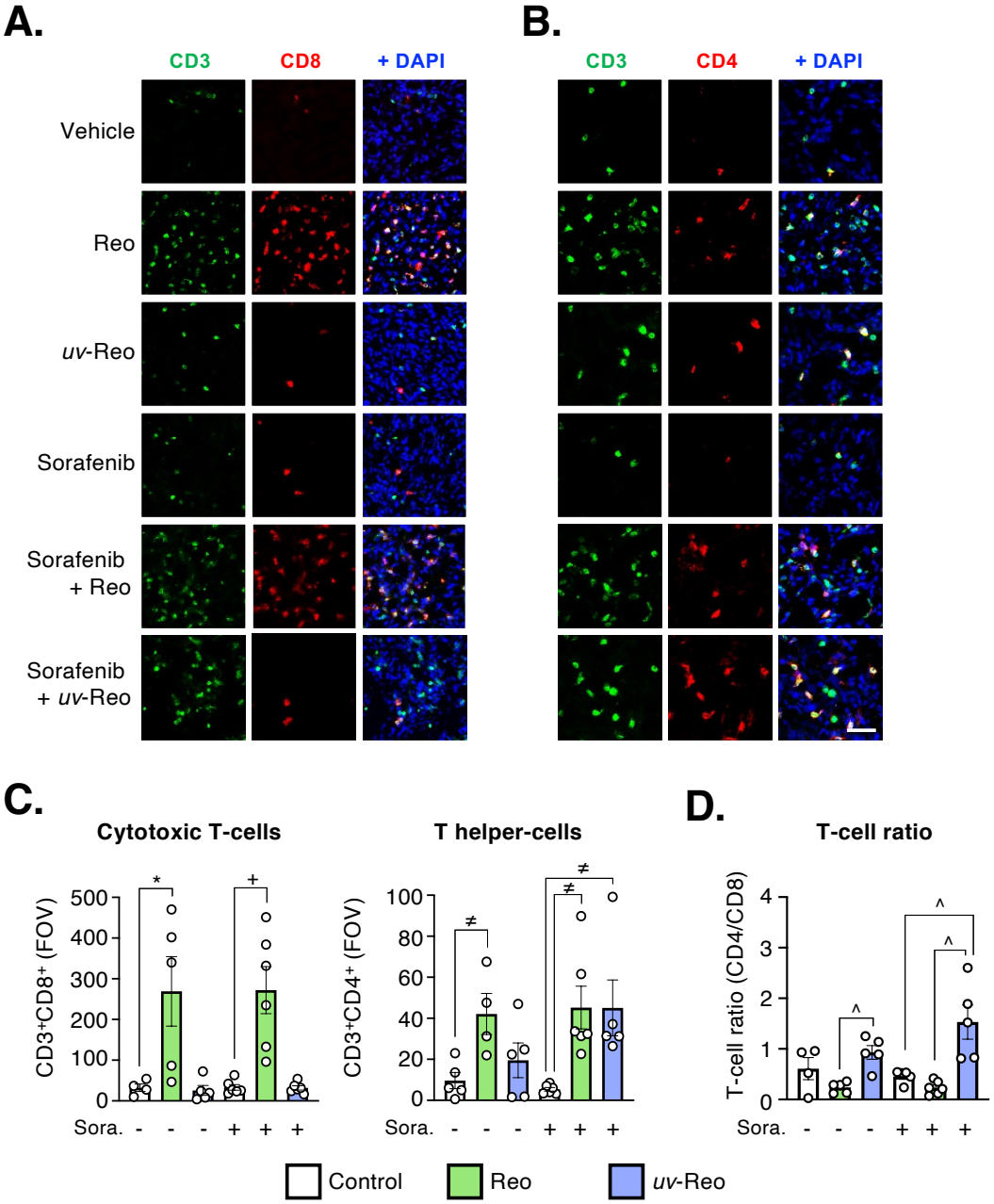
A.
CD3
CD8
+ DAPI
Vehicle
Reo
uv-Reo
Sorafenib
Sorafenib + Reo
Sorafenib + uv-Reo
B.
CD3
CD4
+ DAPI
C.
Cytotoxic T-cells
CD3+CD8+ (FOV)
500
400
300
200
100
0
Sora. - - - + + +
T helper-cells
CD3+CD4+ (FOV)
100
80
60
40
20
0
Sora. - - - + + +
D.
T-cell ratio
T-cell ratio (CD4/CD8)
4
3
2
1
0
Sora. - - - + + +
Control
Reo
uv-Reo

Figure 2. $CD4^+$ T-helper cells, but not $CD8^+$ CTLs, accumulate in murine hepatocellular carcinomas responding to the combination of *uv*-reovirus and sorafenib. Cryosections from murine HCC tumors treated with Reo/*uv*-Reo alone ($1x10^7$ pfu) and in combination with sorafenib (10 mg/Kg), sampled during the "*Therapy-phase*", were immunofluorescently labelled for (**A**) CTLs ($CD3^+CD8^+$) and (**B**) T_H-cells ($CD3^+CD4^+$). (**C**) The abundance was of CTLs and T_H-cells was quantified in random fields of view (F.O.V.) obtained by confocal microscopy and the ratio of the two cell types was determined (**D**). (Scale bar = 50 µm; * $p<0.05$, ≠ $p<0.01$, + <0.001, ^ <0.0001; n = 5 mice per condition).

Figure 3

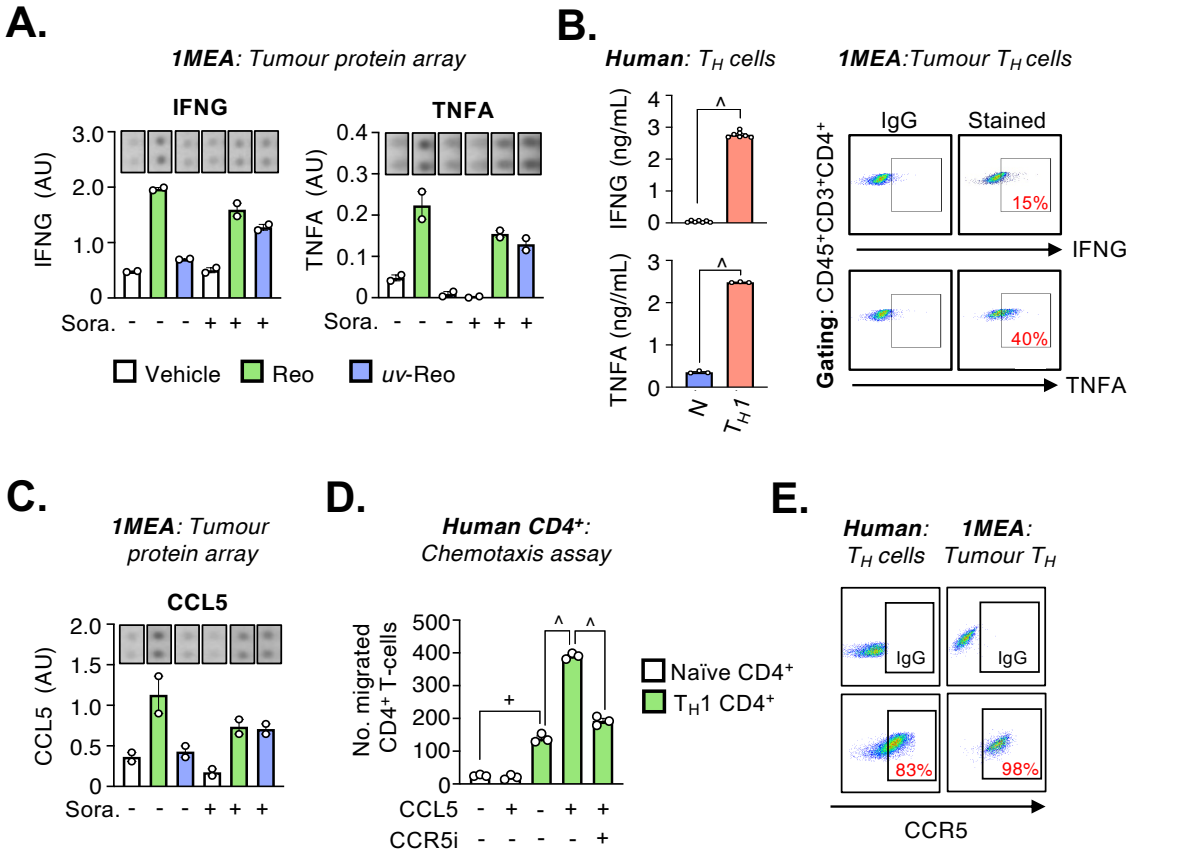
A.
1MEA: Tumour protein array
IFNG
TNFA
IFNG (AU)
TNFA (AU)
Sora.
Vehicle
Reo
uv-Reo
B.
Human: TH cells
1MEA:Tumour TH cells
IFNG (ng/mL)
TNFA (ng//mL)
N
TH1
IgG
Stained
15%
40%
IFNG
TNFA
Gating: CD45+CD3+CD4+
C.
1MEA: Tumour protein array
CCL5
CCL5 (AU)
D.
Human CD4+: Chemotaxis assay
No. migrated CD4+ T-cells
Naïve CD4+
TH1 CD4+
CCL5
CCR5i
E.
Human: TH cells
1MEA: Tumour TH
IgG
83%
98%
CCR5

Figure 3. Treatment of murine HCC tumors with *uv*-Reo/sorafenib therapy elicits at $CD4^+$ T_H1-cell response. (**A**) Cytokine array analysis of pooled protein extracts generated from murine HCC tumors treated with Reo/*uv*-Reo alone ($1x10^7$ pfu) or in combination with sorafenib (10 mg/Kg), data are shown for IFNG and TNFA (samples pooled from 5 mice per treatment group). (**B**) Quantification of IFNG and TNFA in supernatants from unstimulated naive human $CD4^+$ T-cells or following three days of activation in the presence of antibodies against CD3/CD28 and the cytokines IL2 (50 U/mL) and IL12 (10 ng/mL). (**C**) Cytokine array data generated as described in 'A' showing data for CCL5. (**D**) Chemotaxis assay comparing migration of naive or T_H1-activated human $CD4^+$ T-cells towards recombinant human CCL5 (100 ng/mL) in the presence of the CCR5 inhibitor 'Maraviroc' (1 μM) or vehicle (DMSO). (**E**) Flow cytometric data showing expression of CCR5 on the surface of human $CD4^+$ T_H1-cells (*left*) and $CD45^+CD3^+CD4^+$ T_H-cells in murine HCC tumors treated with *uv*-Reo/sorafenib therapy (*right*) (Sora. = Sorafenib, CCR5i = Maraviroc; * $p<0.05$, ≠ $p<0.01$, + <0.001, ^ <0.0001).

Figure 4

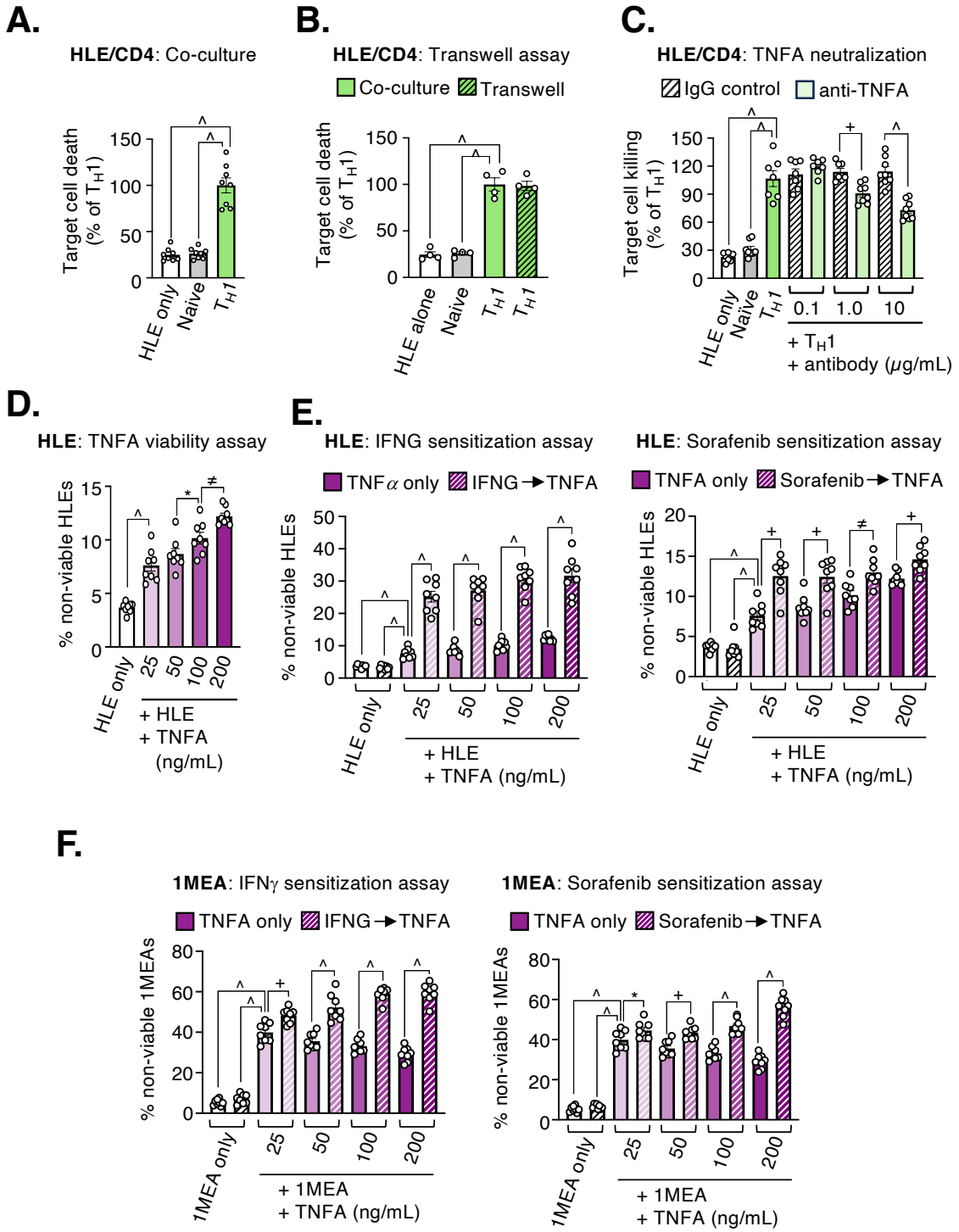
A.
HLE/CD4: Co-culture
Target cell death (% of TH1)
HLE only
Naive
TH1
B.
HLE/CD4: Transwell assay
Co-culture
Transwell
Target cell death (% of TH1)
HLE alone
Naive
TH1
TH1
C.
HLE/CD4: TNFA neutralization
IgG control
anti-TNFA
Target cell killing (% of TH1)
HLE only
Naive
TH1
0.1
1.0
10
+ TH1
+ antibody (μg/mL)
D.
HLE: TNFA viability assay
% non-viable HLEs
HLE only
25
50
100
200
+ HLE
+ TNFA (ng/mL)
E.
HLE: IFNG sensitization assay
TNFα only
IFNG→TNFA
% non-viable HLEs
HLE only
25
50
100
200
+ HLE
+ TNFA (ng/mL)
HLE: Sorafenib sensitization assay
TNFA only
Sorafenib→TNFA
% non-viable HLEs
HLE only
25
50
100
200
+ HLE
+ TNFA (ng/mL)
F.
1MEA: IFNγ sensitization assay
TNFA only
IFNG→TNFA
% non-viable 1MEAs
1MEA only
25
50
100
200
+ 1MEA
+ TNFA (ng/mL)
1MEA: Sorafenib sensitization assay
TNFA only
Sorafenib→TNFA
% non-viable 1MEAs
1MEA only
25
50
100
200
+ 1MEA
+ TNFA (ng/mL)

Figure 4. T_H1-activated $CD4^+$ T-cells exert a TNFA-dependent tumoricidal activity that is enhanced by tumor cell exposure to IFNG or sorafenib. (**A**) Co-culture assay between human HCC cell line 'HLE' in the presence of either naive or T_H1-activated human $CD4^+$ T-cells. HLE target cell viability determined by flow cytometry following incubation overnight. (**B**) Co-culture assay between HLEs and human $CD4^+$ T-cells as described in 'A', but with one additional group in which T-cells and HLE target cells are separated by a tissue culture insert with 0.4 μm pore size. (**C**) Co-culture assay setup as described in (A), but in the presence of increasing concentrations of anti-human TNFA neutralizing antibody or isotype-matched control. (**D**) Human HLE HCC cells were treated with increasing concentrations of recombinant human TNFA overnight and tumor cell viability was then determined by flow cytometry. (**E**) Human HLE HCC cells were pre-treated with rhIFNG (100 U/mL) or sorafenib (7 μM) followed by increasing concentrations of TNFA overnight then tumor cell viability determined by flow cytometry. (**F**) Murine HCC cells '1MEA' were treated overnight with increasing concentrations of rmTNFA alone or following pre-treatment with rmIFNG (100 U/mL) or sorafenib (7 μM) then tumor cell viability was determined by flow cytometry (* $p<0.05$, ≠ $p<0.01$, + <0.001, ^ <0.0001; n = 4 – 8 per condition).

Figure 5

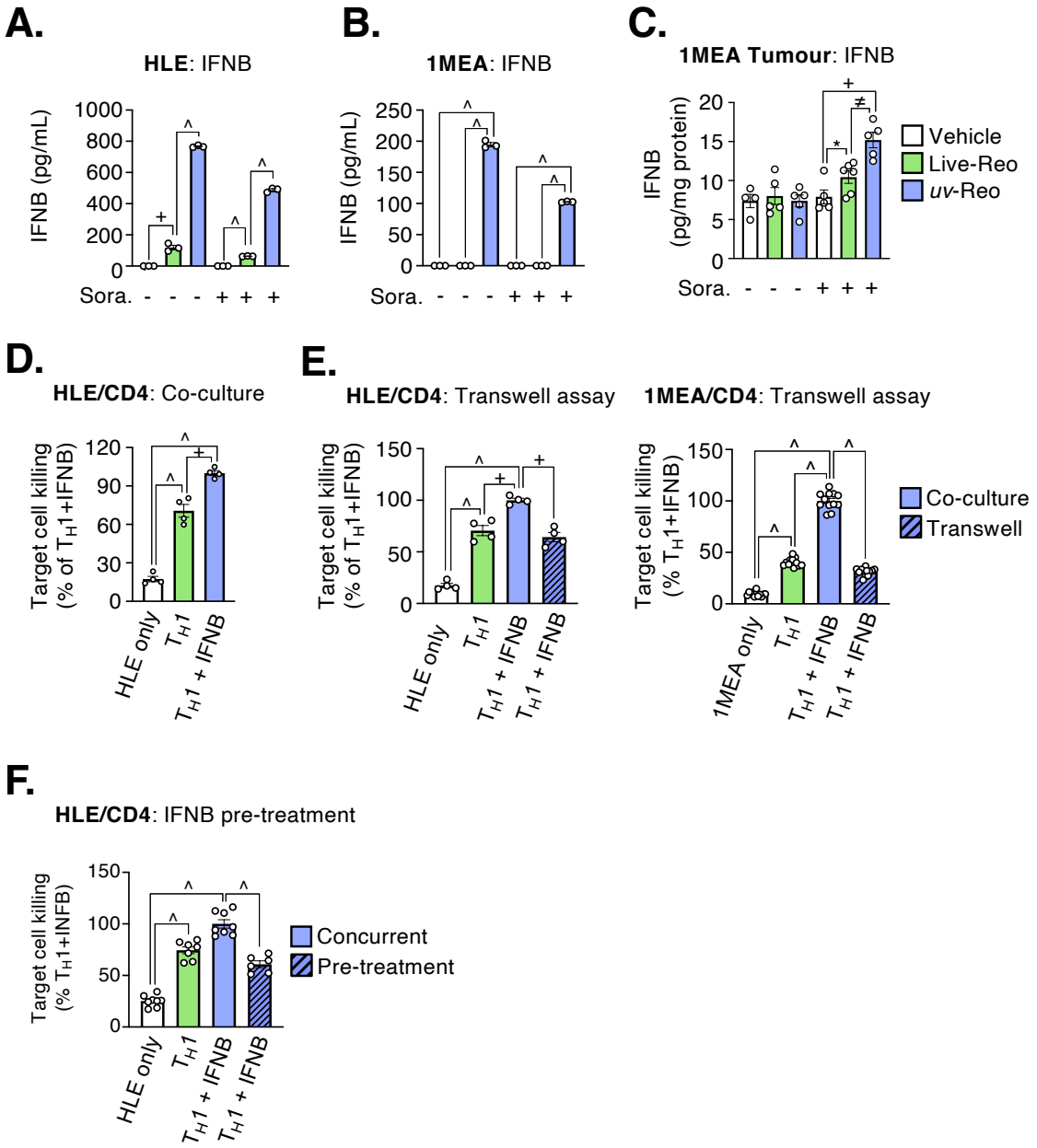
A.
HLE: IFNB
IFNB (pg/mL)
1000
800
600
400
200
0
Sora. - - - + + +
B.
1MEA: IFNB
IFNB (pg/mL)
250
200
150
100
50
0
Sora. - - - + + +
C.
1MEA Tumour: IFNB
IFNB (pg/mg protein)
20
15
10
5
0
Sora. - - - + + +
Vehicle
Live-Reo
uv-Reo
D.
HLE/CD4: Co-culture
Target cell killing (% of TH1+IFNB)
120
90
60
30
0
HLE only
TH1
TH1 + IFNB
E.
HLE/CD4: Transwell assay
Target cell killing (% of TH1+IFNB)
150
100
50
0
HLE only
TH1
TH1 + IFNB
TH1 + IFNB
1MEA/CD4: Transwell assay
Target cell killing (% TH1+IFNB)
150
100
50
0
1MEA only
TH1
TH1 + IFNB
TH1 + IFNB
Co-culture
Transwell
F.
HLE/CD4: IFNB pre-treatment
Target cell killing (% TH1+INFB)
150
100
50
0
HLE only
TH1
TH1 + IFNB
TH1 + IFNB
Concurrent
Pre-treatment

Figure 5. IFNB expression is preferentially induced by *uv*-Reo in HCC cells and elicits a proximity-dependent mode of tumor cell killing in T_H1-activated $CD4^+$ T-cells. Human (**A**) and murine (**B**) HCC cells were treated with Reo/*uv*-Reo (2 pfu/cell) alone or in combination with sorafenib (7 μM) overnight and IFNB was quantified in supernatants by ELISA (n = 3). (**C**) Total tumor lysates were generated from murine HCC tumors, grown *in vivo,* treated with either live- or *uv*-reo alone ($1x10^7$ pfu) and in combination with sorafenib (10 mg/kg) or vehicle then IFNB was quantified by ELISA (n = 5). (**D**) Co-culture assay between human HLE HCC cells and either naive or T_H1-activated $CD4^+$ T-cells with or without rhIFNB (500 ng/mL). Target HCC cell viability was determined by flow cytometry following overnight incubation. (**E**) Co-culture assay using human (*left*) and murine (*right*) cells setup as described in (D), but with one additional group in which T-cells and target HCC cells were separated by a tissue culture insert with a 0.4 μm pore size. (**F**) Co-culture assay between human HLE HCC cells and either naive or T_H1-activated $CD4^+$ T-cells with or without rhIFNB (500 ng/mL) added concurrently with T-cell seeding or added to HCC cells prior T-cell seeding (Sora. = Sorafenib; * $p<0.05$, ≠ $p<0.01$, + <0.001, ^ <0.0001; n = 4 – 8 per condition).

Figure 6

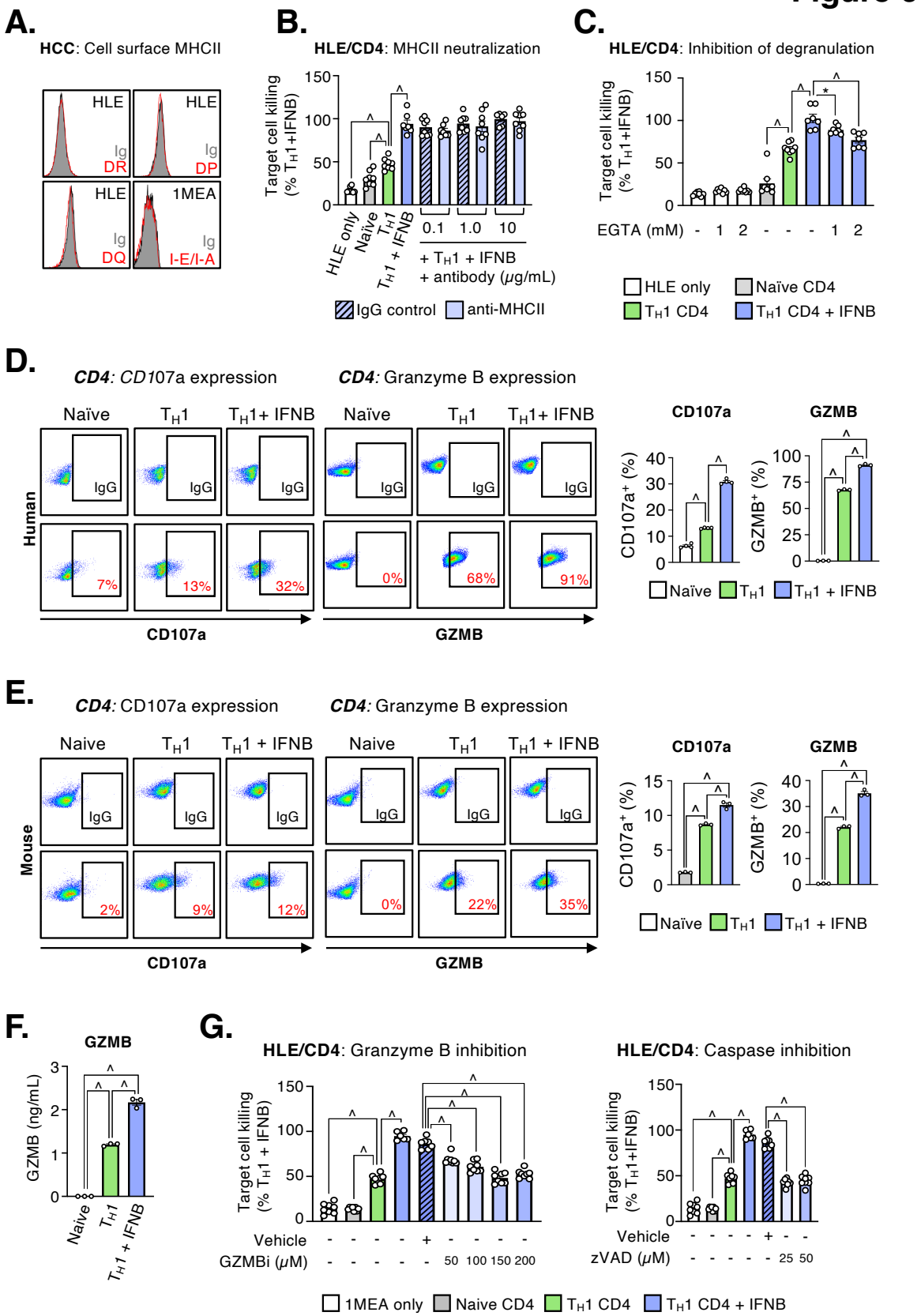
A.
HCC: Cell surface MHCII
HLE
Ig
DR
HLE
Ig
DP
HLE
Ig
DQ
1MEA
Ig
I-E/I-A
B.
HLE/CD4: MHCII neutralization
Target cell killing (% TH1+IFNB)
150
100
50
0
HLE only
Naïve
TH1
TH1 + IFNB
0.1
1.0
10
+ TH1 + IFNB
+ antibody (μg/mL)
IgG control
anti-MHCII
C.
HLE/CD4: Inhibition of degranulation
Target cell killing (% TH1+IFNB)
EGTA (mM) - 1 2 - - - 1 2
HLE only
Naïve CD4
TH1 CD4
TH1 CD4 + IFNB
D.
CD4: CD107a expression
CD4: Granzyme B expression
Naïve
TH1
TH1+ IFNB
Human
IgG
7%
13%
32%
0%
68%
91%
CD107a
GZMB
CD107a
GZMB
CD107a+ (%)
GZMB+ (%)
Naïve
TH1
TH1 + IFNB
E.
CD4: CD107a expression
CD4: Granzyme B expression
Naive
TH1
TH1 + IFNB
Mouse
IgG
2%
9%
12%
0%
22%
35%
CD107a
GZMB
CD107a
GZMB
CD107a+ (%)
GZMB+ (%)
Naïve
TH1
TH1 + IFNB
F.
GZMB
GZMB (ng/mL)
Naïve
TH1
TH1 + IFNB
G.
HLE/CD4: Granzyme B inhibition
Target cell killing (% TH1 + IFNB)
Vehicle - - - - + - - - -
GZMBi (μM) - - - - - 50 100 150 200
HLE/CD4: Caspase inhibition
Target cell killing (% TH1+IFNB)
Vehicle - - - - + - -
zVAD (μM) - - - - - 25 50
1MEA only
Naive CD4
TH1 CD4
TH1 CD4 + IFNB

Figure 6. IFNB induces an antigen and perforin-independent, granzyme B-dependent mode of tumoricidal activity in T_H1-activated $CD4^+$ T-cells. (**A**) Flow cytometric analysis of cell surface MHCII proteins on human (HLE) and murine (1MEA) HCC cell lines. (**B**) Co-culture assay between human HLE HCC cells and either naive or T_H1-activated $CD4^+$ T-cells in the presence of rhIFNB with or without anti-MHCII neutralizing antibodies or isotype matched control. (**C**) Co-culture assay between human HLE HCC cells and either naive or T_H1-activated $CD4^+$ T-cells alone, with rhIFNB and in the presence of increasing concentrations of degranulation inhibitor 'EGTA'. Flow cytometric analysis of cell surface degranulation marker CD107a and intracellular expression of GZMB using human (**D**) and murine (**E**) naive or T_H1-activated $CD4^+$ T-cells treated overnight with rIFNB (mouse 50 ng/mL; human 500 ng/mL). (**F**) The presence of GZMB was quantified in supernatants from human naive or T_H1-activated $CD4^+$ T-cells treated with or without rhIFNB overnight. (**G**) Co-culture assay between human HLE HCC cells and either naive or T_H1-activated $CD4^+$ T-cells with or without rhIFNB (500 ng/mL) overnight in the presence of increasing concentrations of a GZMB inhibitor, pan-caspase inhibitor or vehicle. (GZMBi = GZMB inhibitor; * $p<0.05$, ≠ $p<0.01$, + <0.001, ^ <0.0001; n = 3 – 8 per condition).

Figure S1

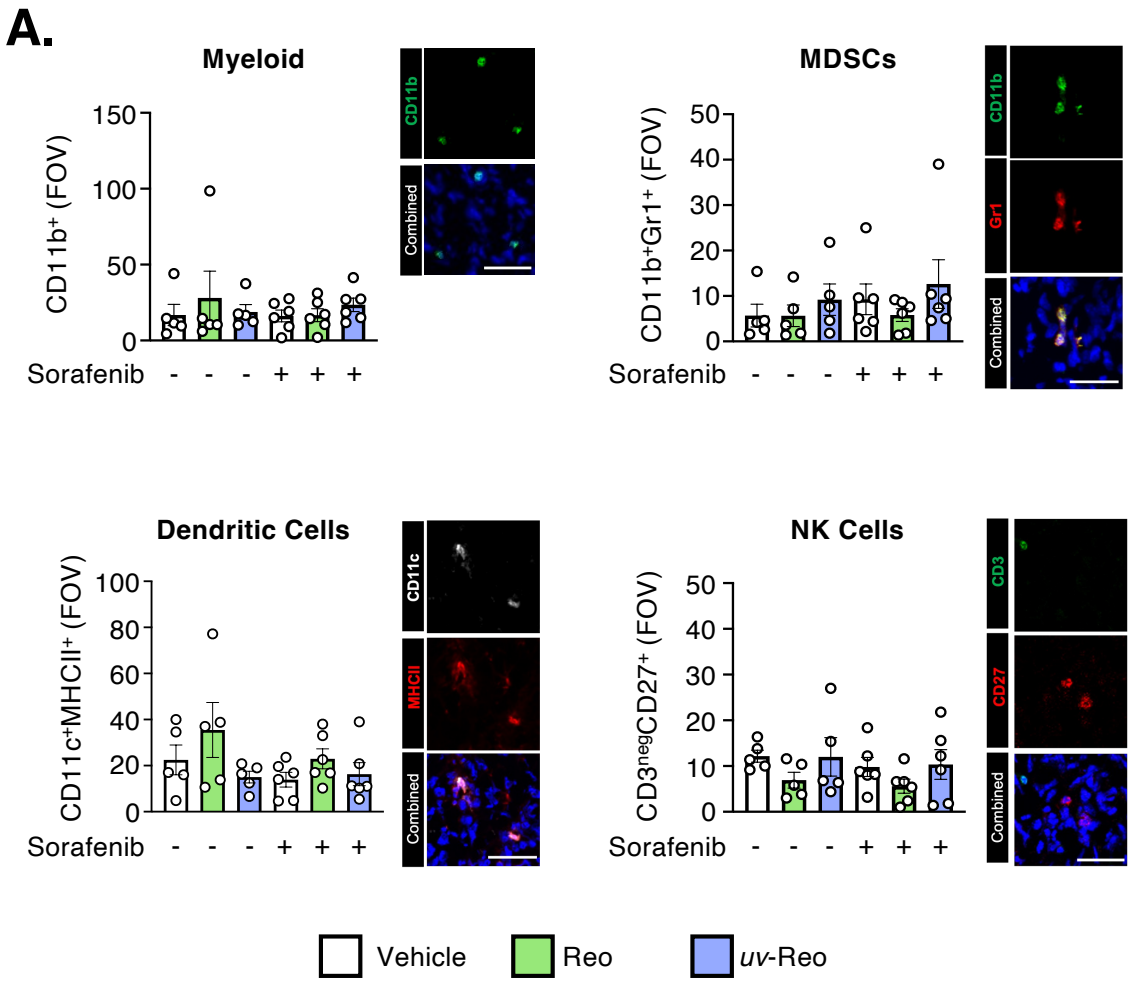
A.
Myeloid
CD11b+ (FOV)
150
100
50
0
Sorafenib - - - + + +
CD11b
Combined
MDSCs
CD11b+Gr1+ (FOV)
50
40
30
20
10
0
Sorafenib - - - + + +
CD11b
Gr1
Combined
Dendritic Cells
CD11c+MHCII+ (FOV)
100
80
60
40
20
0
Sorafenib - - - + + +
CD11c
MHCII
Combined
NK Cells
CD3negCD27+ (FOV)
50
40
30
20
10
0
Sorafenib - - - + + +
CD3
CD27
Combined
Vehicle
Reo
uv-Reo

Figure S1. Leukocyte abundance in syngeneic mouse hepatocellular carcinomas is largely unaffected by treatment with either reovirus or sorafenib. Cryosections were taken from murine HCC tumors grown in syngeneic hosts during the “Therapy-phase” following treatment with either Reo/*uv*-Reo alone ($1x10^7$ pfu) or in combination with sorafenib (7 μM) or vehicle. Tumor cryosections were immunofluorescently labelled for the detection of pan-myeloid cells ($CD11b^+$), MDSCs ($CD11b^+Gr1^+$), dendritic cells ($CD11c^+MHCII^+$) or NK cells ($CD3^{neg}CD27^+$) (n = 5 mice per condition).

Figure S2

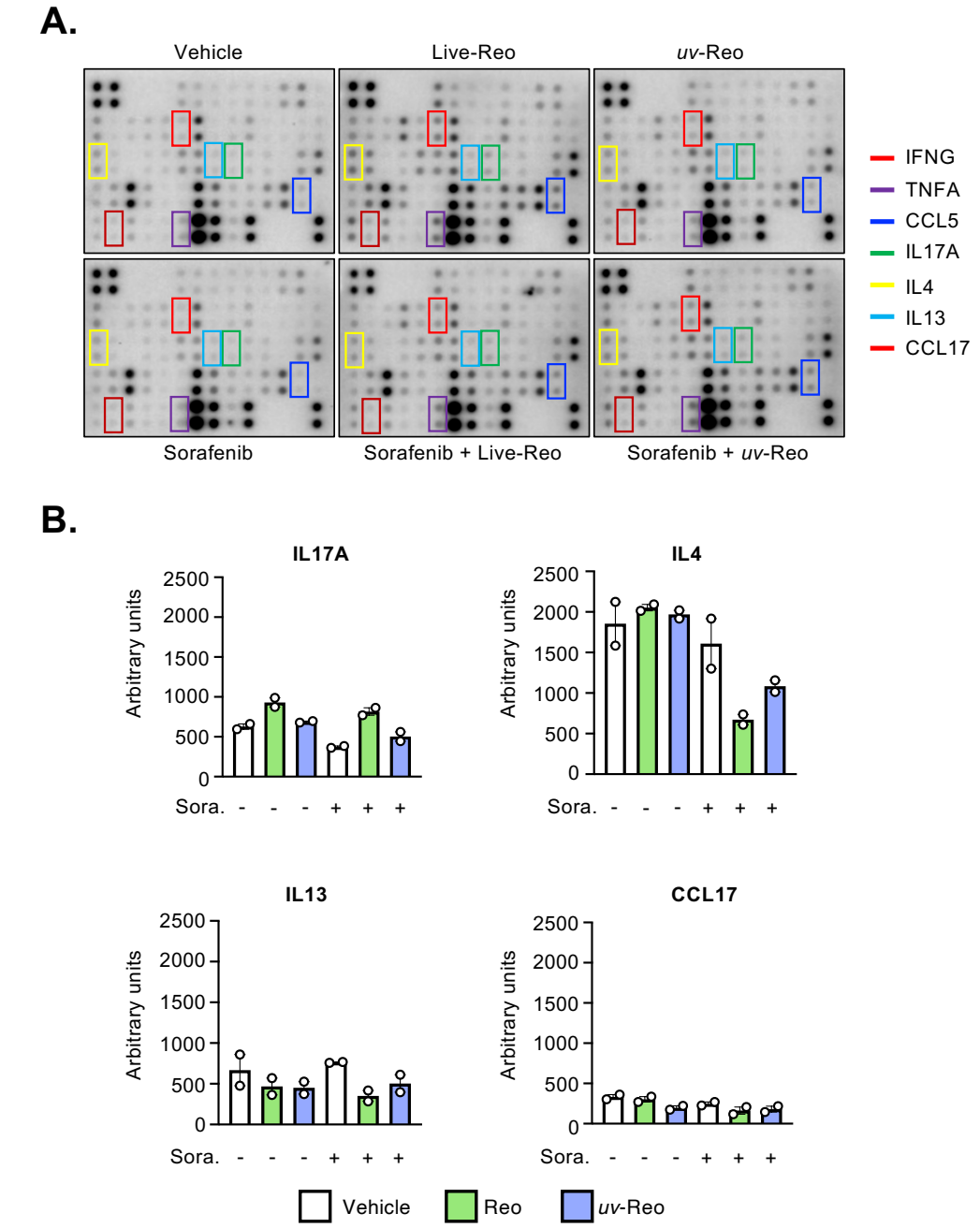
A.
Vehicle
Live-Reo
uv-Reo
Sorafenib
Sorafenib + Live-Reo
Sorafenib + uv-Reo
IFNG
TNFA
CCL5
IL17A
IL4
IL13
CCL17
B.
IL17A
IL4
IL13
CCL17
Arbitrary units
2500
2000
1500
1000
500
0
Sora. - - - + + +
Vehicle
Reo
uv-Reo

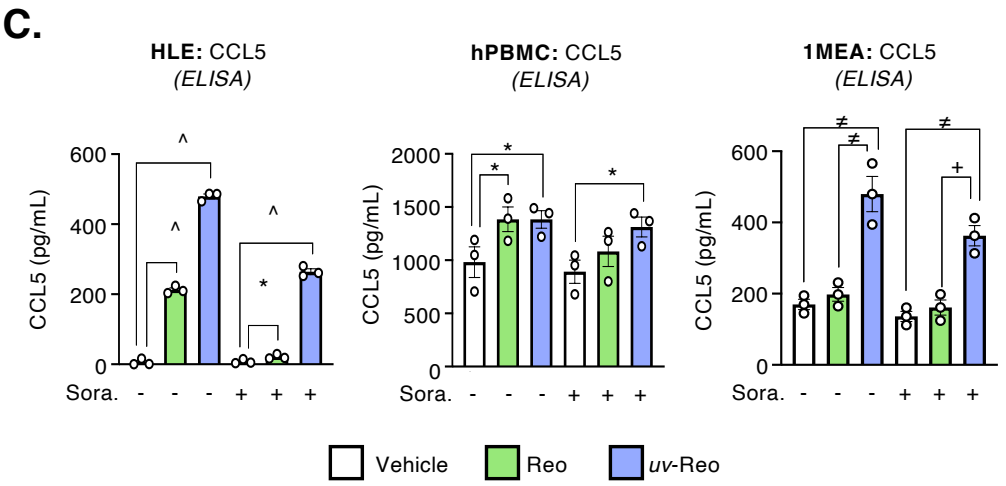
C.
HLE: CCL5
(ELISA)
hPBMC: CCL5
(ELISA)
1MEA: CCL5
(ELISA)
CCL5 (pg/mL)
600
400
200
0
2000
1500
1000
500
Sora. - - - + + +
Vehicle
Reo
uv-Reo

Figure S2. Reovirus alone or in combination with sorafenib induced an intra-tumoral cytokine profile inconsistent with the recruitment or either T_H2 or T_H17 $CD4^+$ T-cell. (**A**) Images of cytokine arrays generated using pooled total tumor protein extracts from murine 1MEA HCC tumors grown in syngeneic host collected during the "Therapy-phase" following treatment with Reo/*uv*-Reo alone ($1x10^7$ pfu) or in combination with sorafenib (10 mg/Kg) or vehicle. Cytokines of interest are highlighted. (**B**) Semi-quantitative data for T_H2 and $T_H17$cytokines from protein arrays shown in 'A'. (Pooled lysates were generated from 4 – 5 mice per treatment group and each cytokine semi-quantitatively measured in duplicate) (**C**) CCL5 was quantified in supernatants from human HLE monolayer cells (*left*), human PBMCs (*centre*), and mouse 1MEA cells grown as spheroids (*right*) following overnight treatment with Reo/*uv*-Reo alone (2 pfu/cell) or in combination with sorafenib (7 μM) (* $p<0.05$, ≠ $p<0.01$, + <0.001, ^ <0.0001; n = 3 per condition).

Figure S3

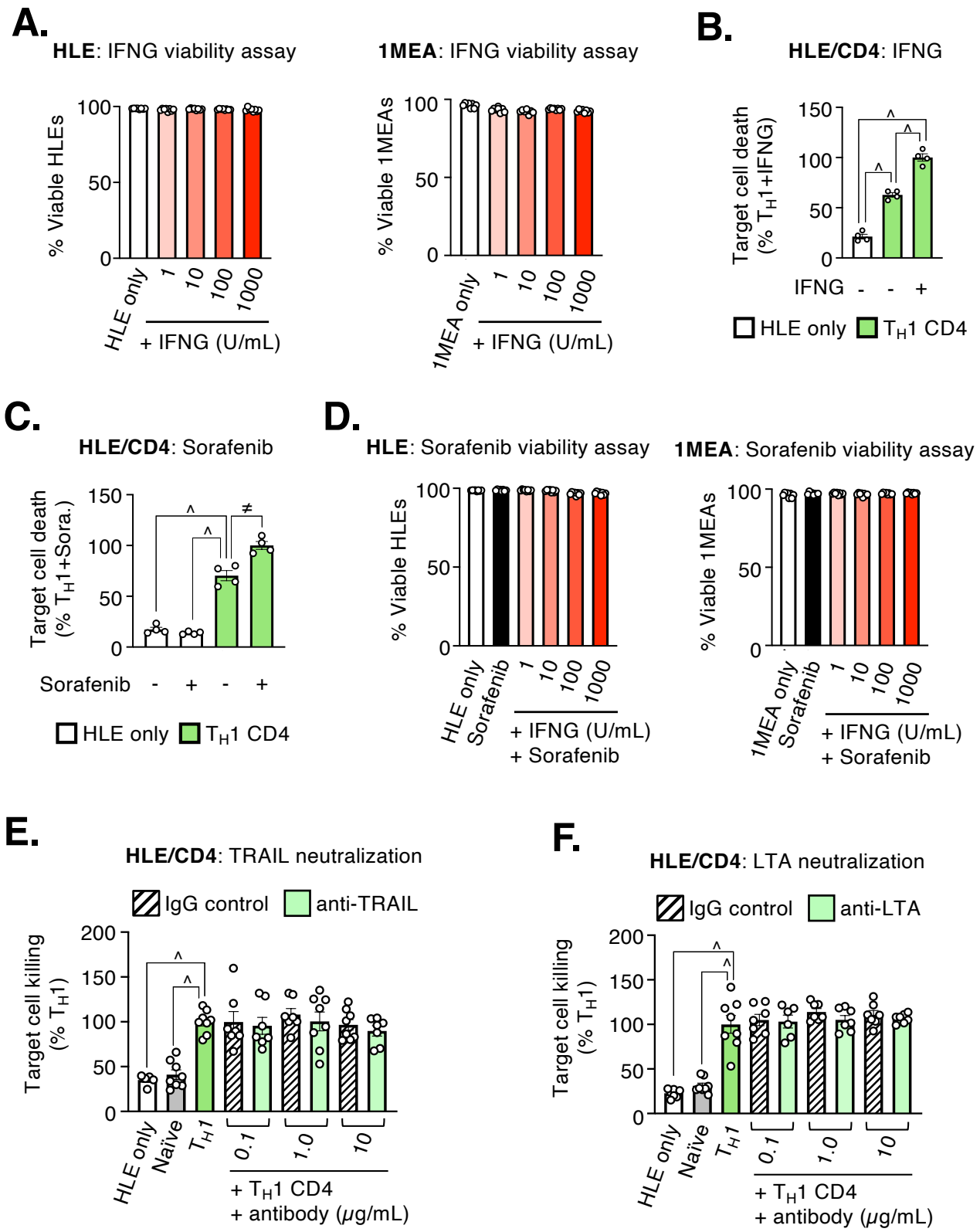
A.
HLE: IFNG viability assay
% Viable HLEs
100
50
0
HLE only
1
10
100
1000
+ IFNG (U/mL)
1MEA: IFNG viability assay
% Viable 1MEAs
1MEA only
B.
HLE/CD4: IFNG
Target cell death (% TH1+IFNG)
150
IFNG - - +
HLE only
TH1 CD4
C.
HLE/CD4: Sorafenib
Target cell death (% TH1+Sora.)
Sorafenib - + - +
D.
HLE: Sorafenib viability assay
Sorafenib
+ IFNG (U/mL)
+ Sorafenib
1MEA: Sorafenib viability assay
E.
HLE/CD4: TRAIL neutralization
IgG control
anti-TRAIL
Target cell killing (% TH1)
200
Naïve
TH1
0.1
1.0
10
+ TH1 CD4
+ antibody (μg/mL)
F.
HLE/CD4: LTA neutralization
anti-LTA

Figure S3. The tumoricidal activity of T_H1-cells against HCC cells is enhanced by pre-treatment with IFNG or sorafenib and killing is mediated by neither TRAIL nor LTA. (A) Human and murine HCC cells were treated with increasing concentration of rIFNG overnight and tumor cell viability determined by flow cytometry. (**B**) Co-culture assay between human HLE HCC cells pre-treated with or without rhIFNG (100 U/mL) and T_H1-activated $CD4^+$ T-cells. Target HCC cell viability determined by flow cytometry following overnight incubation (**C**) Co-culture assay between human HCC cells pre-treated with or without sorafenib (7 μM) and T_H1-activated $CD4^+$ T-cells. Target HCC cell viability was determined by flow cytometry following overnight incubation. (**D**) Human and murine HCC cells pre-treated with sorafenib (7 μM) prior to exposure to increasing concentrations of rIFNG overnight. HCC viability was determined by flow cytometry. Co-culture assays were performed overnight between human HLE HCC cells and either naive or T_H1-activated $CD4^+$ T-cells in the presence of increasing concentrations of neutralizing antibodies against either TRAIL (**E**) or LTA (**F**) and target HCC cell viability was determined by flow cytometry (* $p<0.05$, ≠ $p<0.01$, + <0.001, ^ <0.0001; n = 4 – 8 per condition).

Figure S4

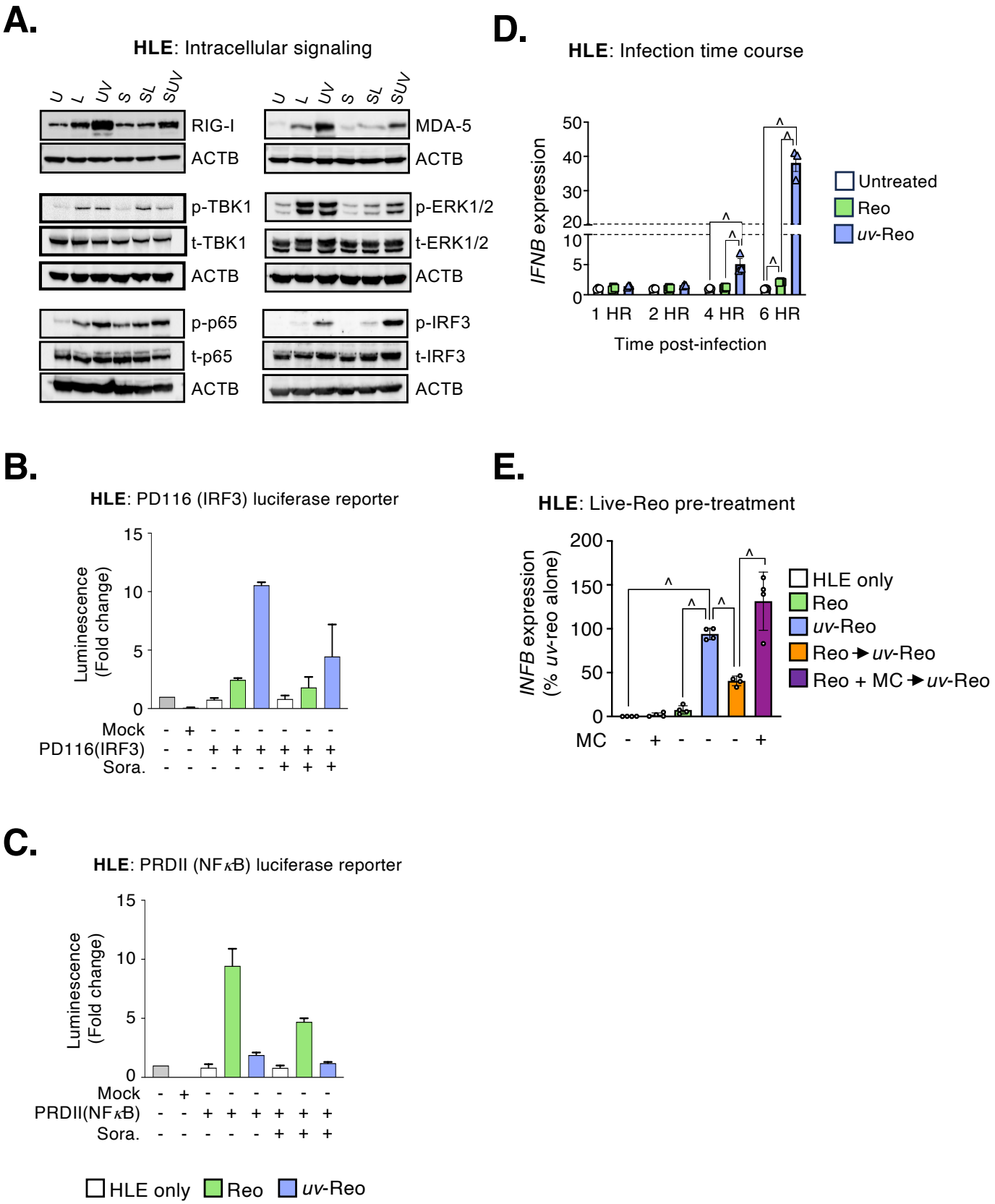
A.
HLE: Intracellular signaling
U L UV S SL SUV
RIG-I
ACTB
MDA-5
ACTB
p-TBK1
t-TBK1
ACTB
p-ERK1/2
t-ERK1/2
ACTB
p-p65
t-p65
ACTB
p-IRF3
t-IRF3
ACTB
B.
HLE: PD116 (IRF3) luciferase reporter
Luminescence (Fold change)
Mock
PD116(IRF3)
Sora.
C.
HLE: PRDII (NFκB) luciferase reporter
Luminescence (Fold change)
Mock
PRDII(NFκB)
Sora.
HLE only
Reo
uv-Reo
D.
HLE: Infection time course
IFNB expression
1 HR
2 HR
4 HR
6 HR
Time post-infection
Untreated
Reo
uv-Reo
E.
HLE: Live-Reo pre-treatment
INFB expression (% uv-reo alone)
MC
HLE only
Reo
uv-Reo
Reo → uv-Reo
Reo + MC → uv-Reo

Figure S4. Differential induction of IFNB by Reo/*uv*-Reo in HLE cells arises from the expression of a virus-derived virulence factor. (**A**) Human HLE HCC cells were treated with Reo/*uv*-Reo (2 pfu/cell) overnight and total protein lysates examined by Western blot, under denaturing and reducing conditions, for activation of downstream signalling pathways. HLE HCC cells were transfected with plasmid luciferase reporter constructs containing IRF3 (**B**) NF*k*B (**C**) and IRF3 responsive elements from the IFNB promoter and treated as describe in 'A' before luciferase activity was quantified. (**D**) HLE HCC cells were treated with Reo/*uv*-Reo (2 pfu/cell), RNA samples were collected at the indicated time-points post-infection and qRT-PCR was performed to quantify changes in the expression of *IFNB* over time. (**E**) HLE HCC cells were infected with Reo/*uv*-Reo alone (2 pfu/cell) or with Reo followed by *uv*-Reo six hours later in the presence or absence of 2'-C-methylcytidine (30 μM). Following incubation overnight, RNA was extracted and the expression of *IFNB* was determined by qRT-PCR (* $p<0.05$, ≠ $p<0.01$, + <0.001, ^ <0.0001; n = 3 per condition).

Figure S5

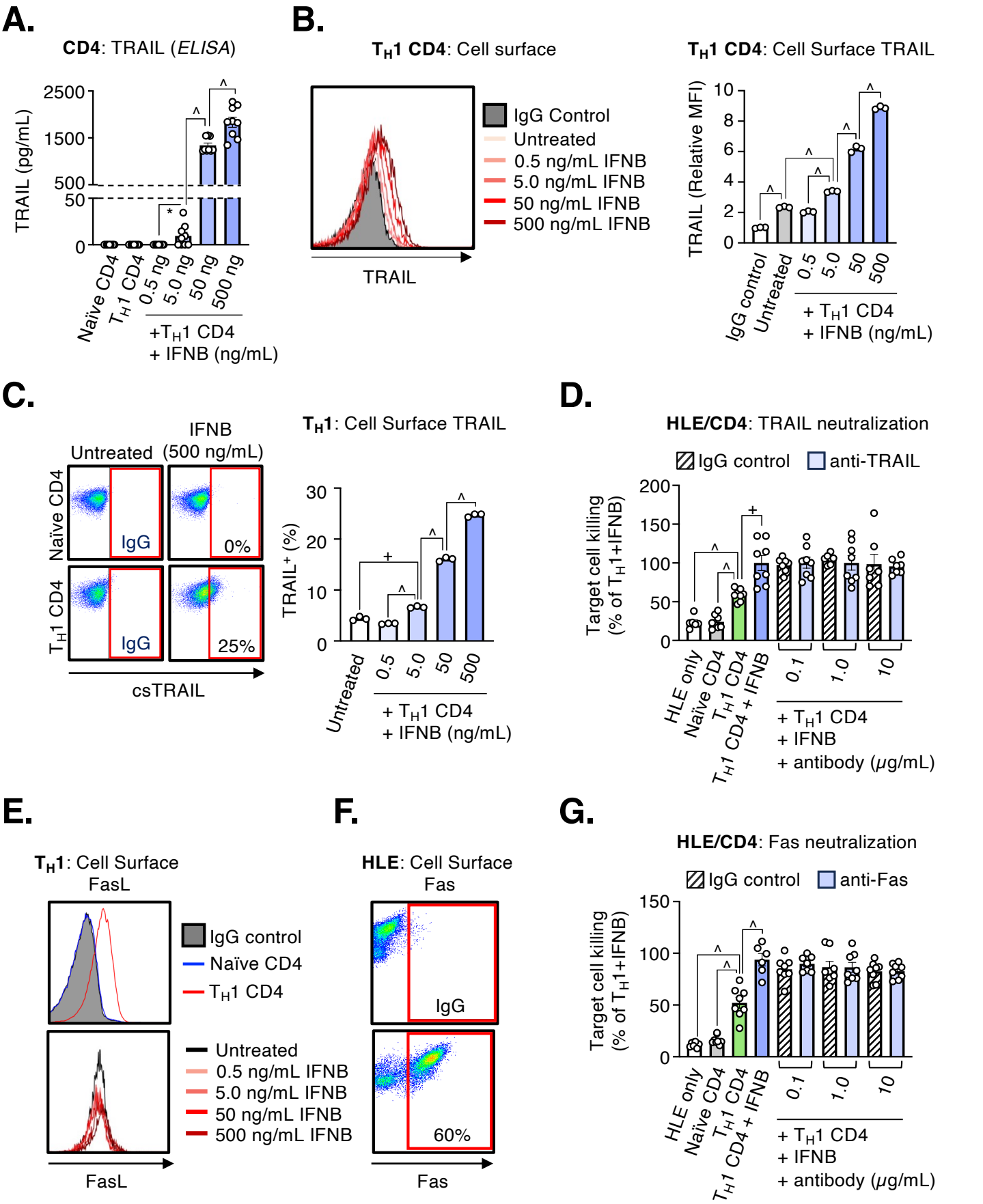
A.
CD4: TRAIL (ELISA)
TRAIL (pg/mL)
2500
1500
500
50
0
Naïve CD4
TH1 CD4
0.5 ng
5.0 ng
50 ng
500 ng
+TH1 CD4
+ IFNB (ng/mL)
B.
TH1 CD4: Cell surface
IgG Control
Untreated
0.5 ng/mL IFNB
5.0 ng/mL IFNB
50 ng/mL IFNB
500 ng/mL IFNB
TRAIL
TH1 CD4: Cell Surface TRAIL
TRAIL (Relative MFI)
IgG control
Untreated
0.5
5.0
50
500
+ TH1 CD4
+ IFNB (ng/mL)
C.
IFNB
Untreated
(500 ng/mL)
Naïve CD4
TH1 CD4
IgG
0%
25%
csTRAIL
TH1: Cell Surface TRAIL
TRAIL+ (%)
Untreated
+ TH1 CD4
+ IFNB (ng/mL)
D.
HLE/CD4: TRAIL neutralization
IgG control
anti-TRAIL
Target cell killing
(% of TH1+IFNB)
HLE only
Naïve CD4
TH1 CD4
TH1 CD4 + IFNB
0.1
1.0
10
+ TH1 CD4
+ IFNB
+ antibody (μg/mL)
E.
TH1: Cell Surface
FasL
IgG control
Naïve CD4
TH1 CD4
Untreated
0.5 ng/mL IFNB
5.0 ng/mL IFNB
50 ng/mL IFNB
500 ng/mL IFNB
FasL
F.
HLE: Cell Surface
Fas
IgG
60%
Fas
G.
HLE/CD4: Fas neutralization
IgG control
anti-Fas
Target cell killing
(% of TH1+IFNB)
HLE only
Naïve CD4
TH1 CD4
TH1 CD4 + IFNB
0.1
1.0
10
+ TH1 CD4
+ IFNB
+ antibody (μg/mL)

Figure S5. The tumoricidal activity of T_H1-activated $CD4^+$ T-cells treated with IFNB is not mediated by TRAIL or FasL/Fas. (**A**) T_H1-activated $CD4^+$ T-cells were treated with increasing concentrations of rhIFNB overnight and the concentration of soluble TRAIL was measured in supernatants by ELISA (n = 9). (**B** - **C**) T_H1-activated $CD4^+$ T-cells were treated overnight as described in 'A' and cell surface expression of TRAIL was quantified by flow cytometry (n = 3). (**D**) Co-culture assay between human HLE HCC cells and either naive of T_H1-activated $CD4^+$ T-cells with or without rhIFNB in the presence of increasing concentrations of anti-human TRAIL neutralizing antibody. Following incubation overnight, target HCC cell killing was determined by flow cytometry (n = 8). (**E**) Human HLE HCC cells were treated with increasing concentrations of rhIFNB overnight and cell surface expression of FasL was quantified by flow cytometry (n = 3). (**F**) Expression of FasL receptor – Fas – on human HLE HCC cells was confirmed by flow cytometry (n = 3). (**G**) Co-culture assay between human HLE HCC cells and either naive or T_H1-activated $CD4^+$ T-cells, with or without IFNB, in the presence of increasing concentrations of anti-human Fas neutralizing antibody or isotype matched control (csTRAIL = cell surface TRAIL; * $p<0.05$, ≠ $p<0.01$, + <0.001, ^ <0.0001; n = 8).

Figure S6

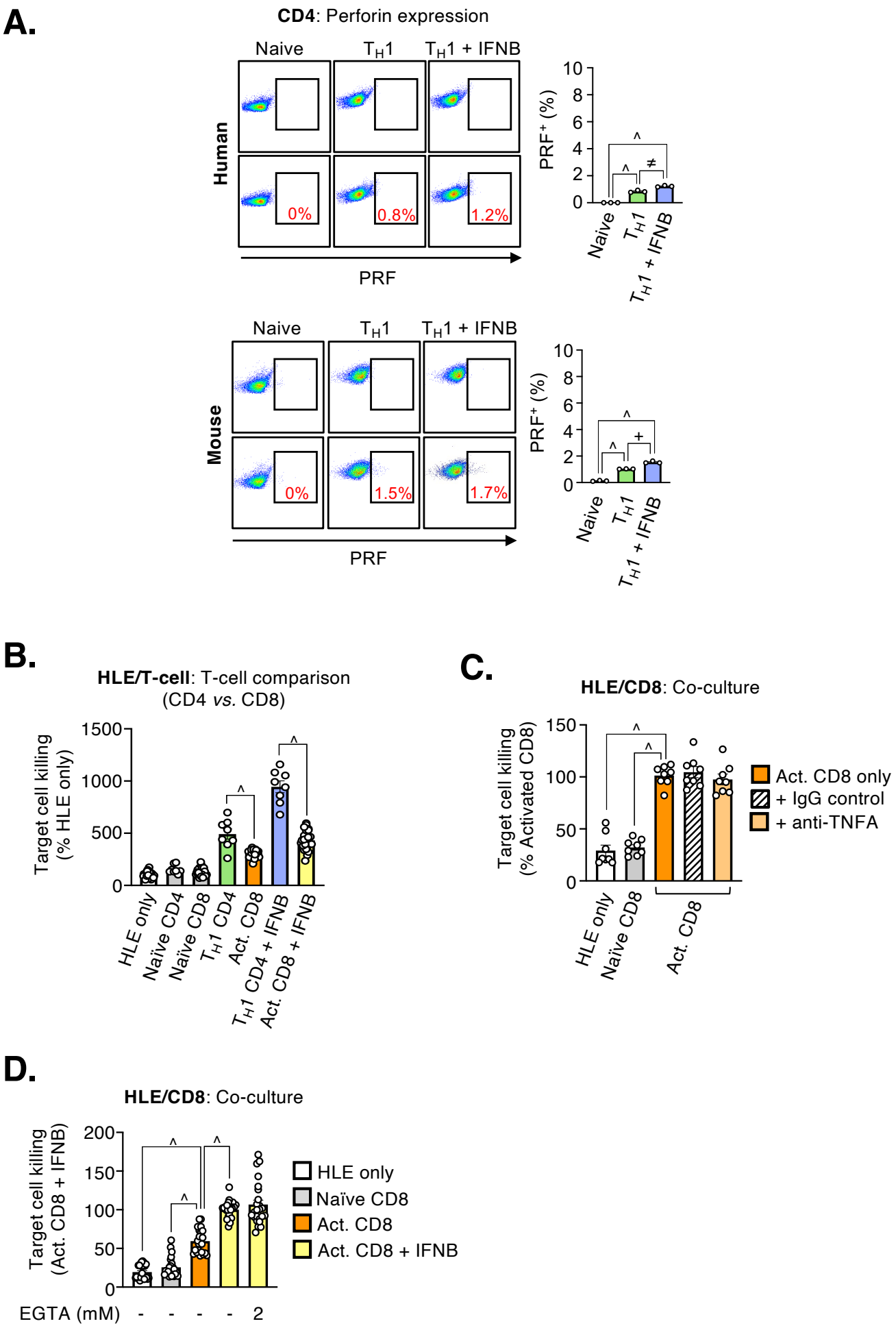
A.
CD4: Perforin expression
Naive
TH1
TH1 + IFNB
Human
0%
0.8%
1.2%
PRF
PRF+ (%)
Naive
TH1
TH1 + IFNB
Mouse
0%
1.5%
1.7%
B.
HLE/T-cell: T-cell comparison
(CD4 vs. CD8)
Target cell killing
(% HLE only)
HLE only
Naïve CD4
Naïve CD8
TH1 CD4
Act. CD8
TH1 CD4 + IFNB
Act. CD8 + IFNB
C.
HLE/CD8: Co-culture
Target cell killing
(% Activated CD8)
Act. CD8 only
+ IgG control
+ anti-TNFA
HLE only
Naïve CD8
Act. CD8
D.
HLE/CD8: Co-culture
Target cell killing
(Act. CD8 + IFNB)
HLE only
Naïve CD8
Act. CD8
Act. CD8 + IFNB
EGTA (mM) - - - - 2

Figure S6. $CD8^+$ T-cells display inferior antigen-independent tumoricidal activity against HCC cells compared with $CD4^+$ T_H-cells and use neither TNFA nor degranulation as their principal mode of killing. (A) The proportion of perforin-expressing human (*top*) and murine (*bottom*) $CD4^+$ T-cells was quantified by intracellular flow cytometry using either naïve, T_H1-activated, or T_H1-activated T-cells in the presence of rIFNB (n = 3). (**B**) Co-culture assay between human HLE HCC cells and either naive or activated T-cells in the presence of absence of rhIFNB (500 ng/mL). (**C**) Co-culture assay between human HLE HCC cells and naive or activated $CD8^+$ T-cells in the presence of anti-human TNFA neutralizing antibody (10 µg/mL) or isotype matched control. (**D**) Co-culture assay between human HLE HCC cells and either naive or activated $CD8^+$ T-cells with or without rhIFNB (500 ng/mL) in the presence of the degranulation inhibitor 'EGTA' (2 mM). The degree of target cell killing was determined in all co-culture assay by flow cytometry following incubation overnight. (**D**) Comparison of $CD3^+CD4^+$ and $CD3^+CD8^+$ T-cell ratio in cryosections taken from murine 1MEA HCC tumors grown in syngeneic hosts and treated for two weeks with either Reo/*uv*-Reo alone ($1x10^7$ pfu) or in combination with sorafenib (7 µM) or vehicle (Act. = activated, Sora. = sorafenib; * $p<0.05$, ≠ $p<0.01$, + <0.001, ^ <0.0001; n = 8 per condition).